npj Precision Oncology

https://doi.org/10.1038/s41698-026-01489-9

Article in Press

Olverembatinib, a novel BCR-ABL tyrosine kinase inhibitor, exhibits anti-tumor activity and synergizes with gemcitabine in pancreatic ductal adenocarcinoma

Received: 17 July 2025

Accepted: 10 May 2026

Cite this article as: Xia, Z., Lin, R., Luo, F. *et al.* Olverembatinib, a novel BCR-ABL tyrosine kinase inhibitor, exhibits anti-tumor activity and synergizes with gemcitabine in pancreatic ductal adenocarcinoma. *npj Precis. Onc.* (2026). https://doi.org/10.1038/s41698-026-01489-9

Zengfei Xia, Runduan Lin, Fan Luo, Qiuyun Luo, Jing Yang, Shan Shi, Yan Li, Jiaxing Cao, Miaozhen Qiu, Lin Zhang, Wenlong Guan & Dajun Yang

Title page

Olverembatinib, a novel BCR-ABL tyrosine kinase inhibitor, exhibits anti-tumor activity and synergizes with gemcitabine in pancreatic ductal adenocarcinoma

Zengfei Xia[1#], Runduan Lin[2#], Fan Luo[3#], Qiuyun Luo[4#], Jing Yang[1], Shan Shi[1], Yan Li[1], Jiaxing Cao[5], Miaozhen Qiu [6], Lin Zhang[2*], Wenlong Guan[6*], Dajun Yang[1*]

[#] These authors contributed equally to this work.

[*] CORRESPONDENCE

Lin Zhang[*]

Email: zhanglin@sysucc.org.cn;

Wenlong Guan[*]

Email: guanwl@sysucc.org.cn;

Dajun Yang[*]

Email: yangdj@sysucc.org.cn;

Affiliations

[1] Department of Experimental Research, State Key Laboratory of Oncology in South China, Collaborative Innovation Center for Cancer Medicine, Sun Yat- Sen University Cancer Center, Guangzhou, China;

[2] Department of Clinical Laboratory, Sun Yat- Sen University Cancer Center, Guangzhou, China;

[3] Department of Intensive Care Unit, Sun Yat-Sen University Cancer Center, Guangzhou, China;

[4] Cytotherapy Laboratory, The First Affiliated Hospital (Shenzhen People's Hospital), Southern University of Science and Technology, Shenzhen, China;

[5] Department of Surgical Anesthesiology, Sun Yat-Sen University Cancer Center, Guangzhou, China;

[6] Department of Medical Oncology, Sun Yat-Sen University Cancer Center, Guangzhou, China;

Abstract

Pancreatic ductal adenocarcinoma (PDAC) is one of the most lethal diseases with few treatment options. The aberrant activation of SRC PDAC suggests it as a promising therapeutic target. Here, we evaluated the antitumor activity of olverembatinib, a novel multi-target tyrosine kinase inhibitor, as a single agent and in combination with gemcitabine, the standard chemotherapeutic backbone for PDAC treatment. Our results demonstrated that olverembatinib showed a potent anti-tumor effect and significantly enhanced the sensitivity of PDAC to gemcitabine both *in vitro* and *in vivo*. Mechanistically, olverembatinib inhibited SRC/AKT/cMYC signaling pathway, leading to cell cycle arrest, suppression of metastasis, and induction of apoptosis. For combination with gemcitabine, the JAK1-STAT1 might server as an important mechanistic basis of synergy. Clinically, olverembatinib exhibited promising efficacy in patients with advanced PDAC who had failed multiple prior lines of therapies, including gemcitabine-based treatment. These findings suggest that olverembatinib, either as monotherapy or in combination with gemcitabine, represents a promising novel therapeutic strategy for the treatment of PDAC.

Keywords: Olverembatinib; SRC; MYC; Gemcitabine; PDAC

1. Introduction

Pancreatic ductal adenocarcinoma (PDAC), the major pathological subtypes (>90%) of pancreatic cancers[1], is one of the most aggressive malignancies, with a dismal 5-year survival rate of just 3% in metastatic cases[2]. Over the past decade, the standards of care for the treatment of PDAC were quadruplet FOLFIRINOX (5-fluorouracil, leucovorin, irinotecan, and oxaliplatin) and the doublet nab-paclitaxel plus gemcitabine[3-5]. Despite comprehensive genomic profiling, no targeted therapy has proven clinically effective against PDAC. Given the poor prognosis and limited therapeutic options for most patients, novel treatment strategies and sensitize cytotoxic regimens is urgently needed.

PDAC comprises characterized mutations with five key genes: KRAS, CDKN2A, CDKN1A, TP53 and SMAD4[6-8]. Several targeted therapies against these mutated genes are currently under clinical investigation for PDAC[9,10]. Beyond genetic alterations, several studies observed elevated SRC protein expression or hyperphosphorylation in over 70% of PDAC samples[11]. SRC could drive PDAC growth by upregulating IGF-1 receptor and promote angiogenesis via ERK1/2/IL-8 signaling[12,13]. In chemoresistance, hyperphosphorylated SRC disrupts DNMT1-BUB3 interaction, reducing the methylation of oncogene promoter, whereas SRC inhibition restores pyroptosis and chemosensitivity[14,15]. These studies demonstrated an SRC-centered network which facilitates PDAC progress and drug resistant. While SRC is a crucial target in pancreatic cancer therapy, monotherapy targeting SRC alone might activated potential bypass pathways which lead to limited antitumor effects. Thus, combining SRC inhibitors with other targeted therapies or using multi-target agent containing SRC target may yield superior antitumor efficacy, reduce the risk of drug resistance and release more potent antitumor efficiency[16,17].

Olverembatinib is an oral, third-generation BCR-ABL1 tyrosine kinase inhibitor (TKI) developed by Ascentage Pharma. It has been approved for treating chronic myelogenous leukemia (CML) with resistance to third-generation BCR-ABL-targeted therapies in China[18].

In solid tumors, olverembatinib significantly suppresses the growth of Gleevec-resistant gastrointestinal stromal tumors (GIST) in preclinical studies and succinate dehydrogenase (SDH)-deficient GIST in an ongoing phase I dose-escalation trial[19,20]. Olverembatinib has a broad target spectrum, including several key oncogenes in PDAC, such as SRC, MAP2K5 and FGFR, which renders it an attractive candidate for monotherapy and combination strategies.

In this study, we evaluated the antitumor efficacy of olverembatinib monotherapy and the combination with gemcitabine in PDAC, and undercover the underlying mechanism. Our results reveal that olverembatinib monotherapy inhibits tumor cell viability, suppressing proliferation and migratory and invasive capacities. What's more, olverembatinib combined with gemcitabine showed more potent synergistic antitumor efficacy while maintaining a favorable safety profile. Importantly, our clinical data further demonstrated that olverembatinib showed encouraging anti-PDAC efficacy in heavily pretreated patients.

These findings demonstrated the potent antitumor efficiency of olverembatinib monotherapy and the combination with gemcitabine might be a promising clinical strategy in PDAC treatment.

2. Results

2.1 Olverembatinib exerts a potent inhibitory effect on cell proliferation in PDAC cells

Among multiple solid tumors cells, the IC50 values of pancreatic cancer cell lines, with the exception of PANC1, ranged from 0.1 μM to 0.01 μM, whereas in most other solid tumor cell lines the IC50 values were above 0.1 μM (Fig. 1A). Then, the CCK8 assays showed that olverembatinib exerted time- and concentration-dependent inhibitory effect (Fig. 1B). The morphological and density changes of pancreatic cancer cells after olverembatinib treatment further validated above findings (Fig. 1C). Considantly, the number of cell colonies significantly decreased with increasing olverembatinib concentration (Fig. 1D). What's more, compared with other TKIs (Dasatinib and Bosutinib), olverembatinib also showed a better inhibition on cell

growth under the same concentration (Supplementary Fig. 1A). Furtherly, EdU labeling directly showed the proportion of proliferating cells with active DNA replication among the total cell population progressively decreased with olverembatinib treatment (Fig. 1E-F). These findings demonstrate that olverembatinib potently inhibits the proliferative capacity of PDAC cells.

2.2 Olverembatinib induces cell cycle arrest and apoptosis in PDAC cells

To further characterize the underlying mechanisms of olverembatinib, its effects on cell cycle and apoptosis of PDAC cell were examined. Cell cycle analysis revealed that olverembatinib treatment significantly induced both G1 and G2/M phase arrest, and markedly reduced S phase populations compared to blank control (Fig. 2A-B). Key cell cycle regulators, including Cyclin D1 and CDK4, were also effectively suppressed by olverembatinib (Fig. 2C-D).

For apoptosis, olverembatinib treatment induced significantly higher apoptosis rates compared to blank control, with effects increasing over concentration (Fig. 2E-F). Compared with other TKIs (Dasatinib and Bosutinib), olverembatinib treatment group had higher percentage of apoptosis cells under the same concentration (Supplementary Fig. 1B). What's more, the percentage of dead PDAC cells was significantly elevated after olverembatinib treatment (Fig. 2G-H). Together, these data indicated that olverembatinib exerts anti-tumor effects through cell cycle arrest and robust inducement of apoptosis.

2.3 Olverembatinib inhibits invasion, migration and upregulates the ROS level in the PDAC cells

Pancreatic cancer is highly aggressive for its propensity of metastasis. The wound healing assay showed that the wound size in the olverembatinib group was larger than in the control group in all PDAC cells (Fig. 3A-B). Further transwell assay revealed the migration and invasion ability of cancer cell was significantly decreased with olverembatinib treatment (Fig. 3C-E). What's more, compared with other TKIs (Dasatinib and Bosutinib), olverembatinib also showed an obvious advantage on the inhibition of migration and invasion ability of cancer cell under the

same concentration (Supplementary Fig. 1C-D). Then, the western blot of EMT markers showed significantly downregulation of N-cad, Vimentin and Snail proteins and upregulation of the epithelial adhesion protein E-cad after olverembatinib treatment (Fig. 3F).

Pancreatic cancer cells exhibit highly malignant characteristics which leading to increased production of highly reactive oxygen species (ROS) during ATP synthesis in mitochondria. To investigate whether olverembatinib regulates intracellular oxidative levels, DCFH-DA, a biomarker for ROS level, was detected by flow cytometry. The results showed that under olverembatinib treatment induced a progressive rise in ROS levels with increased intracellular DCF fluorescence intensity (Fig. 3G-H). NRF2, a critical molecule in the intracellular antioxidant system, was also downregulated by olverembatinib in a concentration-dependent manner (Fig. 3I). Furthermore, the link between increased ROS and apoptosis was validated by using the ROS inducer, and increasing apoptosis of PDAC cells were observed in ROS inducer 5 treatment group (Supplemental Fig. 2A). With above findings, ROS might be a median between the olverembatinib and the anti-tumor apoptosis of PDAC. These results indicated the potent ability of olverembatinib to inhibit cell migration and invasion and induce high intracellular ROS levels in pancreatic cancer cells which contribute to cell apoptosis.

2.4 Olverembatinib inhibits the phosphorylation of SRC, leading to suppression of the phosphorylation of AKT and promoting the degradation of MYC

To further investigate the underlying anti-tumor mechanism of olverembatinib, RNAseq were applied for PANC1 and ASPC1 and pathway enrichment analyses were conducted on all target genes of olverembatinib (Fig. 4A). These targeted genes were primarily involved in peptidyl-tyrosine phosphorylation, protein autophosphorylation, and positive regulation of the MAPK cascade, which are related to tyrosine phosphorylation and MAPK pathway regulation (Fig. 4B). In Molecular Function (MF), they were mainly enriched in functions associated with protein tyrosine kinase activity and protein serine/threonine kinase activity (Fig. 4B). What's more, the PPI analysis of these targeted genes showed the core role of SRC among the interaction network

(Fig. 4C). The TCGA-PDAC cohort also showed higher expression level of SRC and MYC gene in tumor group (Fig. 4D-E). Thus, the inhibitory effect of olverembatinib on SRC was firstly verified, and WB results showed the phosphorylation at the SRC Tyr416 site was significantly inhibited by olverembatinib (Fig. 4F), thereby reducing SRC activity levels.

For KEGG, the genes were predominantly enriched in the MAPK signaling pathway, Ras signaling pathway and PI3K/AKT signaling pathway (Fig. 4G). Similarly, in the REACTOME pathway dataset, they were primarily enriched in MAPK family signaling cascades and PI3K/AKT signaling in cancer (Fig. 4G).

To investigate the key downstream signaling pathways that might be affected by the inhibition of SRC phosphorylation by olverembatinib, three potential downstream molecules: ERK1/2, STAT3 and AKT were validified by WB. The results showed that olverembatinib had no significant effect on the expression or phosphorylation levels of ERK1/2 and STAT3 (Fig. 4H-I). However, the phosphorylation levels of AKT were markedly reduced with increasing concentrations of olverembatinib (Fig. 4J). As drug concentrations increased and AKT phosphorylation inhibition intensified, phosphorylation of c-MYC at Thr58 also decreased, which led to reduction of c-MYC stability and increased c-MYC degradation (Fig. 4J).

These findings indicated that with inhibition of SRC phosphorylation, olverembatinib further suppresses AKT phosphorylation, leading to reduced c-MYC phosphorylation, which promotes c-MYC protein instability and degradation, ultimately resulting in decreased expression of downstream pro-tumorigenic genes related to cell proliferation, growth, and EMT. Consequently, olverembatinib exerts anti-tumor effects by inhibiting tumor growth and invasion.

2.5 AKT activation rescue the anti-tumor efficiency of olverembatinib

To investigate the central role of SRC/AKT/MYC axis in the anti-tumor efficiency of olverembatinib, functional rescue assays were performed with AKT activator (SC79). The colony formation showed the inhibition of olverembatinib on cell proliferation was significantly attenuated by SC79 (Fig. 5A). The same as the apoptosis, after added with SC79, the

inducement of apoptosis by olverembatinib was weaken (Fig. 5B). The rescue effect of migration and invasion by SC79 were also significant in three cell lines. SC79 enhanced the migration and invasion of PDAC cells which were inhibited by olverembatinib (Fig. 5C). The wound healing assays further confirmed this finding (Fig. 5D). Those functional rescue results indicated that the AKT axis played an important role in the anti-tumor mechanism of olverembatinib.

2.6 Downregulation of SLC44A4 in PDAC cells after olverembatinib treatment

To further explore the transcriptional changes following olverembatinib treatment, we performed RNA sequencing on PANC1 and ASPC1 (Fig. 6A). We identified upregulated and downregulated genes in pancreatic ductal adenocarcinoma (PDAC) cells after olverembatinib treatment (Fig. 6B). Subsequent enrichment analysis of these differentially expressed genes (DEGs) for BP, MF, Cellular Component (CC) and KEGG pathways revealed that in PANC1 cells, the DEGs were primarily enriched in metabolic processes, cell growth and death, cell motility and signal transduction (Fig. 6C). In ASPC1 cells, the DEGs were mainly involved in cellular processes, biological regulation, carbohydrate metabolism, and signaling molecules and interactions (Fig. 6D). Gene Set Enrichment Analysis (GSEA) showed that in PANC1 cells neuroactive ligand-receptor interactions were activated after drug treatment, while interleukin-4 and interleukin-3 signaling pathways were suppressed. In ASPC1 cells, olfactory receptor activity and olfactory transduction were activated, whereas nonsense-mediated decay (NMD) was inhibited (Fig. 6E).

Additionally, we intersected the upregulated and downregulated genes in both PANC1 and ASPC1 cells after olverembatinib treatment, yielding six commonly upregulated genes and seven commonly downregulated genes (Supplemental Fig. 3A-B). Among these, SLC44A4, CEACAM5, CXCL3, N4BP3, CD22 and GRP132 were highly expressed in tumor tissues (Supplemental Fig. 3C-D). SLC44A4, typically expressed on the apical surface of secretory epithelial cells, has been identified as a novel cell surface target in most pancreatic and gastric cancers[21]. The correlation analysis with SRC expression across multiple pancreatic cancer datasets revealed a positive relationship between SLC44A4 and SRC (Supplemental Fig. 3E). In

the TCGA-PDAC cohort, SLC44A4, CEACAM5 and CXCL3 exhibited negative correlations with most olverembatinib targeted genes (Supplemental Fig. 3F). Cox regression analysis of these genes also indicated that CD22, COL21A1, and GRP132 were associated with favorable prognosis, whereas SLC44A4 was strongly linked to poor prognosis (Supplemental Fig. 3G). Then, the downregulation of SLC44A4 in PDAC cells by olverembatinib were further validated. The qPCR results in cell lines showed a significant lower expression of SLC44A4 after olverembatinib treatment (Supplemental Fig. 3H). In tumor samples from animal models, regardless of whether in xenograft model or endogenous pancreatic cancer model, the downregulation on SLC44A4 of olverembatinib was consistently favorable (Supplemental Fig. 3I-J). These results suggested that olverembatinib might downregulate the expression of several poor-prognosis related genes, particularly SLC44A4, indicating a critical role for SLC44A4 in the therapeutic mechanism of olverembatinib.

2.7 Olverembatinib hinders tumor growth of PDAC cells *in vivo*

To evaluate the antitumor effect of olverembatinib *in vivo*, PANC1 and ASPC1 xenograft tumor models were established in BALB/C nude mice. The olverembatinib treatment could markedly delay the tumor growth compared to the vehicle control *in vivo* (Fig. 7A-F). What's more, the tumor growth inhibition (TGI) of different doses of olverembatinib in mouse xenograft models was calculated. In the PANC1 model, the 40mg/kg group demonstrated significantly higher inhibition efficacy compared to the 20mg/kg group, while no significance in ASPC1 model (Figs. 7G). Meanwhile, there was no significant difference in body weight among the various groups of mice, indicating the high safety of olverembatinib *in vivo* (Figs. 7H). Importantly, the phosphorylation of SRC, AKT and cMYC, the expression levels of EMT markers were also confirmed in the xenograft model by WB. The phosphorylation of SRC, AKT and cMYC were significantly inhibited in the olverembatinib treatment group, and the E-cad was upregulated and N-cad was downregulated after olverembatinib treatment (Figs. 7I). This finding showed the potent antitumor efficiency and high safety of olverembatinib in *vivo*.

2.8 Olverembatinib combined with gemcitabine exerts potent tumor suppression in PDAC

To further verify the synergistic antitumor effects of combination of olverembatinib and gemcitabine, the cell viability, drug induced cell death and cell cycle arrest were performed. The IC50 of gemcitabine of PADC cells were measured using CCK8 and the results showed PANC1 was relatively insensitive to gemcitabine (Fig. 8A). However, the combination significantly suppressed cell growth compared to either agent alone (Fig. 8B-C). The combination index (CI) calculated by CompuSyn were less than 0.6 for the drug combination in all three cell lines, demonstrating that the synergistic antitumor effects of olverembatinib combined with gemcitabine (Fig. 8D).

Furthermore, SYTOX staining was performed on PDAC cells and the highest proportion of dead cells were observed in the combination group, significantly exceeding that of either monotherapy group (Fig. 8E-F). The combination group also exhibited a stronger G1-phase arrest compared to either monotherapy group (Fig. 8G-H). These results further validate the synergistic antitumor effects of olverembatinib combined with gemcitabine from the perspective of cell cycle arrest and tumor cell death induction.

2.9 The role of interferon gamma signaling in the combination of olverembatinib and gemcitabine

To explore the effect of certain gene expression on the sensitivity to chemotherapy, we examined the correlation coefficients between the expression of SRC, AKT and MYC and the IC50 values of gemcitabine, paclitaxel, irinotecan, 5-Fu, and oxaliplatin across 60 cell lines from the CellMiner database. The results revealed a positive trend ($R > 0$) between the expression of SRC, AKT and MYC and the IC50 of gemcitabine (Fig. 9A), indicating that SRC/AKT/MYC might contribute to reduce the efficiency of gemcitabine. To further explored the underlying molecular change between the combination therapy and monotherapy, PANC1 and ASPC1 were treated with blank control, olverembatinib, gemcitabine and combination and sent for RNAseq. We

mainly focused on the DEGs between the combination and gemcitabine, gemcitabine and blank control (Fig. 9B-C). The REACTOME enrichment analysis for the DEGs showed that both DEGs were involved in the interferon gamma signaling (Fig. 9D-G). The GESA analysis showed an interesting finding that the interferon gamma signaling was inactivated in combination therapy compared with gemcitabine monotherapy, while activated in gemcitabine monotherapy compared with blank control (Fig. 9H-K).

Furthermore, we focused on genes which upregulated in both ASPC1 and PANC1 when compared gemcitabine monotherapy with blank control, while downregulated in both ASPC1 and PANC1 when compared combination therapy with gemcitabine monotherapy, and 12 genes were collected (Supplemental Fig. 4A-C). The correlation analysis between the expression of 12 genes and the targeted genes of olverembatinib showed that MFSD2A, RND1, CCL20 and HLA-B showed a positive relationship with SRC expression, besides, the APOL3 and TNFRSF9 also showed a positive relationship with most targeted genes (Supplemental Fig. 4D). What's more, key genes of interferon gamma pathways were also analysed and the heatmap showed that except the MFSD2A and FAM222A, the remain 10 genes which upregulated in gemcitabine monotherapy and the targeted genes were both showed a positive relationship with the key genes of interferon gamma pathways (Supplemental Fig. 4E). These results revealed that the interferon gamma signaling might serve as a key downstream pathway for the synergistic anti-tumor effect of olverembatinib combined with gemcitabine.

2.10 Olverembatinib combined with gemcitabine inhibits PDAC growth *in vivo*

To better simulate the clinical scenario and further validate the efficacy of olverembatinib combined with gemcitabine *in vivo* as observed in vitro, we established two xenograft tumor models in nude mice. Analysis of tumor volume changes revealed no statistically significant difference between the olverembatinib monotherapy group and the gemcitabine monotherapy group in either model. However, the combination group showed significantly smaller tumor volumes compared to either monotherapy group. (Fig. 10A-F). Furthermore, the tumor growth

inhibition (TGI) rates for each treatment group in both models were calculated and the results revealed that the combination group exhibited superior tumor suppression compared to the monotherapy groups (Fig. 10G). Additionally, the changes in mouse body weight across treatment groups were analyzed and we found that the olverembatinib-gemcitabine combination did not induce weight loss, indicating favorable safety profiles for this therapeutic regimen (Fig. 10H-I). The RNAseq analysis suggested the interferon gamma signaling might be an important pathway for the synergistic anti-tumor effect, and the core of the interferon signaling pathway is the activation of STAT1 via JAK kinases. To investigated the role of JAK1-STAT1 axis in the mechanistic basis of synergy, WB were applied for the tumor sample from animal model with different treatment. Interestingly, there was no difference of p-JAK1 level between control and gemcitabine treatment, while decreased in the olverembatinib and completely abolished in the combination group (Fig. 10J). The p-STAT1 level also showed the same trend. Besides, the p-SRC level only significantly inhibited in the olverembatinib and combination group (Fig. 10J). This finding verified the significant efficacy and well-tolerated safety of combination therapy and confirm role of JAK1-STAT1 axis in the synergistic anti-tumor effect of olverembatinib combined with gemcitabine.

2.11 The anti-tumor efficiency of Olverembatinib monotherapy or combined with gemcitabine in endogenous pancreatic cancer model

Considering the dense desmoplastic stroma of subcutaneous models, to more accurately recapitulate the tumor microenvironment and evaluate the efficiency of olverembatinib monotherapy or combination therapy, the endogenous pancreatic cancer model was generated by in situ pancreatic injection of AKT/MYC plasmids (Fig. 11A). The monotherapy results showed a consistent result as nude mice model, the tumor-bearing pancreas was lighter in olverembatinib group than control without significant body weight change (Fig. 11B-E). The inhibition of phosphorylation of SRC, AKT and cMYC were also verified in the olverembatinib group (Fig. 11F). For combination with olverembatinib and gemcitabine, a consistent trend was also

observed. Compared with control, both olverembatinib and gemcitabine monotherapy showed a significant antitumor effect, and the combination group showed a better tumor suppression with the smallest tumor/body rate compared with monotherapy groups (Fig. 11G-I). What's more, the JAK1-STAT1 axis was also confirmed in the combination therapy group as observed in the nude mice model. The p-JAK1 level was slightly inhibited by olverembatinib and no change in the gemcitabine group while almost completely inhibited in the combination group (Fig. 11J). The results in the endogenous pancreatic cancer model further validated the findings in the cell lines and nude animal models.

2.12 Olverembatinib exhibited promising efficacy in patients with advanced PDAC who had failed multiple prior lines of therapies including gemcitabine-based treatment

We observed a long progression-free survival in a PDAC patient with lung metastasis who participated in a phase I clinical trial evaluating the anti-tumor efficacy of olverembatinib (NCT03594422) (Fig. 12A-B). Standard treatments, including albumin-bound paclitaxel combined with gemcitabine as first line and FOLFIRINOX regimen as second line, failed in this patient. Since April 2023, olverembatinib was orally administered at 40mg once every other day (QOD) for consecutive 4 weeks each cycle. Though objective response was not achieved, this patient had stable disease (SD) with a progression-free survival of 5.5 months. The disease ultimately progressed in September 2023. The change of lung metastasis and primary tumor tissue between pre- and post-treatment was recorded with the CT image, and the primary tumor site and lung metastasis both remained stable during the Olverembatinib treatment (Fig. 12C). The long PFS observed in this patient revealed that olverembatinib might serve as a treatment option for patients who had failed multiple prior lines of therapies, but further exploration, especially combination with other anti-tumor therapies, is needed.

3.Discussion

Olverembatinib is a novel multi-target tyrosine kinase inhibitor (TKI), exploring the efficacy of

olverembatinib in pancreatic cancer holds potential clinical value. In this study, we investigated the efficacy of olverembatinib monotherapy and the combination with gemcitabine in pancreatic cancer and validated these findings in xenograft and orthotopic animal models.

Across multiple cancer cell lines, we evaluated its tumor-suppressive effects and found that it exhibited the strongest antitumor activity in pancreatic cancer. Given the highly aggressive nature of pancreatic cancer, we further investigated its impact on invasiveness[22], and the results showed the potent inhibition of cancer cell invasiveness by olverembatinib, consistent with prior reports that SRC inhibition disrupts E-Cadherin expression via FAK interference[23]. Additionally, due to the abnormally active metabolic activity in pancreatic cancer, intracellular ROS levels exist in a fragile equilibrium[24]. Flow cytometry analysis showed the ROS upregulation induced by olverembatinib, potentially contributing to anti-tumor effects. In animal models, we found dose-dependent tumor growth inhibition without significant changes in mouse body weight across tested doses, confirming its potent anti-tumor efficiency and favorable safety. Especially, potent tumor growth inhibition also observed in endogenous pancreatic cancer model, indicating the well drug delivery of olverembatinib penetrating the dense desmoplastic stroma. This comprehensive study highlights olverembatinib's potent inhibition on proliferation and metastatic ability and in pancreatic cancer with effective drug delivery, while maintaining a safe therapeutic window.

Highly activated SRC in pancreatic cancer cells confer a highly aggressive phenotype. Prior literature reported that SRC promoted hepatocellular carcinoma progression through STAT3 activation[25]. Additionally, SRC phosphorylates and activates the PI3K/AKT pathway, enhancing tumor cell proliferation and growth[26]. In breast cancer, SRC binds to EGFR and phosphorylates its Y845 site, subsequently activating the MEK/ERK1/2 pathway to boost tumor cell migration and invasiveness[27]. Our KEGG analysis of SRC-associated pathways yielded consistent findings. We performed WB on potential downstream effectors of SRC, including AKT, STAT3, and ERK1/2, and the results revealed that while olverembatinib markedly inhibited SRC phosphorylation, it did not significantly alter the phosphorylation levels of STAT3

or ERK1/2. However, AKT phosphorylation was substantially reduced. The functional rescue assays with AKT activator further validated the important role of AKT in the anti-tumor effects of olverembatinib. Thus, AKT inhibition may represent a key downstream mechanism following SRC suppression.

cMYC, a well-characterized oncoprotein, translates into the nucleus to promote the expression of genes associated with tumor progression. cMYC knockout significantly suppresses the growth of KRAS-mutant pancreatic cancer cells, while its overexpression enhances metastasis in pancreatic cancer[28-30]. Immunohistochemical analyses reveal negligible cMYC expression in normal tissues, whereas 38% of pancreatic tumor tissues exhibit cMYC positivity[30]. In terms of cMYC protein regulation, early studies on RAS-mutant fibroblasts identified that the RAF-MEK1/2-ERK1/2 pathway, activated by RAS, phosphorylates cMYC at S62 (pS62), stabilizing the protein[31]. Following S62 phosphorylation, AKT phosphorylation further phosphorylates cMYC at T58 (pT58) through GSK3β[32-34]. The pS62 and pT58 modifications are critical for cMYC stability and loss of pT58 triggers FBXW7 E3 ligase-mediated degradation of cMYC[32]. In our study, after observing olverembatinib-induced suppression of AKT phosphorylation, both pT58 and cMYC protein levels decreased significantly upon AKT inhibition. Thus, olverembatinib's inhibition of SRC phosphorylation primarily impacts the AKT/cMYC axis, leading to reduced AKT phosphorylation, diminished cMYC T58 phosphorylation, increased cMYC instability and proteasomal degradation.

Olverembatinib, compared to other highly selective SRC-targeting drugs, exhibits broader target spectrum. SRC interacts with ERBB2/ERBB3, forming heterocomplexes to stabilize the ERBB2/ERBB3 signaling axis, thereby enhancing tumor cell proliferation[35]. SRC, FYN, and YES can be activated by PDGFR via two autophosphorylated tyrosine sites (Y579/Y581) in its juxtamembrane domain[36,37], and the PY934 of PDGFR is phosphorylated and activated by SRC, promoting PDGF-mediated mitogenesis[38]. Thus, SRC forms an interactive network with molecules like ERBB2, YES, and PDGFR, all of which are olverembatinib targets. SLC44A4 is normally expressed on the apical surface of secretory epithelial cells and has now been identified

as a novel cell surface target in the majority of pancreatic and gastric cancers. Furthermore, our RNAseq analysis and qPCR for PDAC cell lines and tumor sample treated with olverembatinib found that the expression of SLC44A4 was significantly downregulated by olverembatinib. This broad inhibition of SRC-centric signaling circuits may underlie olverembatinib's superior anti-tumor efficacy.

Currently, gemcitabine-based chemotherapy remains the first-line treatment for pancreatic cancer. Our CCK8 assays and CI index calculations demonstrated synergistic anti-tumor effects for olverembatinib-gemcitabine combination. Importantly, in our animal experiments, we conducted *in vivo* validation of the synergistic antitumor effects and safety profile of the drug combination. The RNAseq analysis revealed the interferon-gamma signaling pathway was significantly inhibited compared to gemcitabine monotherapy. JAK1-STAT1 axis is the core pathway of interferon-gamma signaling pathway[39]. The WB validation in tumor samples from different animal models showed that the p-JAK1 and p-STAT1 level were almost significantly inhibited by combination therapy while slightly inhibited in olverembatinib and no change in gemcitabine. The synergistically enhance JAK1-STAT1 inhibition might serve as the mechanistic basis of synergy. These findings confirm the favorable safety profile of this combination regimen and the role of JAK1-STAT1 in synergy effect, thereby providing a robust preclinical foundation for subsequent clinical trials.

Above findings revealed the potent inhibition of proliferation and invasion of olverembatinib in PDAC. The directed comparison to existing multi-kinase inhibitors targeting SRC, like Dasatinib and Bosutinib, further clarify the advantage of olverembatinib in the filed of anti-tumor efficiency. What’s more, the board targets property of olverembatinib, especially the SLC44A4 might confer a lower incidence of drug resistance upon it. The tolerability in animal studies and the oral administration highlighting the well safety of olverembatinib, and the potent anti-tumor performances in endogenous pancreatic cancer mode suggested the well drug delivery of olverembatinib overcoming the dense desmoplastic stroma. However, there were some limitations in this study. For a more comprehensive assessment of the antitumor efficacy of the

drug against pancreatic cancer, more genetic diversity among PDAC cell lines were needed for further in-depth investigations. Although patient imaging data are available, the lack of validation in patient-derived xenograft (PDX) animal models and transcriptome sequencing of clinical samples limits further clinical assessment and demonstration, representing a key aspect that requires future investigation and refinement.

In summary, this study systematically investigated the antitumor effects of olverembatinib in pancreatic cancer and demonstrated its efficacy and safety both in preclinical and clinical settings. Mechanistically, we identified the SRC/AKT/MYC signaling axis as the one of the primary mechanisms. Furthermore, we explored and confirmed the synergistic antitumor effects of olverembatinib in combination with gemcitabine in vitro and vivo, and the JAK1-STAT1 might server as an important mechanistic basis of synergy. This combination strategy holds promise for improving outcomes in PDAC, and as a future clinical application and research direction potentially extending the benefits of precision medicine to a broader patient population.

3. Methods

3.1 Cell lines and culture

Four PDAC cell lines, including PANC1, ASPC1, CAPAN1 and BXPC3, were acquired from American Type Culture Collection (ATCC, Manassas, USA) and verified through STR (short-tandem-repeat) profiling. Among these, PANC1 and CAPAN1 cells were maintained in DMEM medium (Gibco, California, USA), whereas ASPC1 and BXPC3 were grown in RPMI 1640 (Gibco, California, USA), supplemented with 10% fetal bovine serum (FBS) and 1% antibiotic mixture, under standard culture conditions of 37°C with 5% CO_2 in a humidified incubator.

3.2 Patients

The CT image data and the clinical information of PDAC patients received Olverembatinib treatment were obtained from the Sun Yat-sen University Cancer center. Written informed consent has been obtained from all participants involved in the study.

3.3 Reagents and antibodies

Olverembatinib was graciously donated by Ascentage Pharma Group (Suzhou, China) with purity ≥ 99%, whereas SC79, ROS inducer 5 (T200879), Bosutinib, Dasatinib and gemcitabine was obtained commercially from TargetMol (Boston, USA). For in vitro studies, both compounds were prepared as 20 mM stock solutions by dissolving in dimethyl sulfoxide (DMSO) and storage at -20°C. Regarding *in vivo* administration, olverembatinib was incorporated into 0.2% hydroxypropyl methylcellulose (HPMC) suspension in sterile water for oral gavage. Gemcitabine was dissolved in sterile water for injection.

The following antibodies were used for the western blot analysis: SRC (L4A1, Mouse mAb), p-SRC (Tyr416, Rabbit mAb), AKT (11E7, Rabbit mAb), p-AKT (Ser473, Rabbit mAb), cMYC (D84C12, Rabbit mAb), p-cMYC (Thr58, Rabbit mAb), CDK4 (D9G3E, Rabbit mAb), CyclinD1 (E3P5S, Rabbit mAb), E-cad (24E10, Rabbit mAb), N-cad (D4R1H, Rabbit mAb) , Snail (C15D3, Rabbit mAb), Vimentin (D21H3, Rabbit mAb), GAPDH (D16H11, Rabbit mAb), NRF2 (D1Z9C, Rabbit mAb), ERK1/2 (137F5, Rabbit mAb), p-ERK1/2 (Thr202/Tyr204, Rabbit mA), STAT1 (1F7C6, Mouse mAb), p-STAT1 (Tyr701, Rabbit mAb), JAK1 (3H7A8, Mouse mAb), p-JAK-1 (Tyr1034/1035, Rabbit mAb), STAT3 (D3Z2G, Rabbit mAb) and p-STAT3 (Tyr705, Rabbit mAb). Above primary antibodies were purchased from the Cell Signaling Tech (CST, Massachusetts, USA) or (Proteintech, Chicago, USA). The second antibody were Goat anti Mouse Ig-G-HRP and Goat anti Rabbit IgG-HRP from Santa Cruz (Santa Cruz (Texas, USA).

3.4 Cell viability and cell growth assay

Cell viability was assessed using the Cell Counting Kit-8 (Dojindo, Japan). Cells were seeded in 96-well plates at a density of 6 to 8 × 10^3 cells per well and treated with drugs at indicated concentrations for 24h, 36h and 72 h. Following treatment, cells were incubated with CCK-8 reagent for 1.5 h at 37 °C. Absorbance was measured at 450 nm using a microplate reader. The

drug inhibition curves and the IC50 values were generated and calculated in GraphPad Prism software version 8.0 (GraphPad Inc., La Jolla, California, USA).

To assess the clone formation capability, 700 cells were plated into each well of a 6-well plate and different concentrations of drugs were added to the culture medium. Continue culturing for 14 days, the cells were stained with crystal violet for 15 min and washed with PBS. The colony images in each well were captured and the numbers of colonies were calculated via Image J software.

In EdU assay, PDAC cells were seeded at 5×10^4 cells/well in 6-well plates and exposed to different drug concentrations. After 24 hours of treatment, cell proliferation was assessed using the BeyoClick™ EdU Cell Proliferation Kit (Beyotime Biotechnology, Shanghai, China) following the recommended protocol. Imaging was performed promptly at 100× magnification with an inverted microscope (Nikon, Japan) to document proliferating cells.

3.5 Cell cycle arrest and apoptosis analysis

Cell Cycle Detection Kit (KeyGen, Nanjing, China) was used to detect the cell cycle progression of CRC cells according to the instruction. A density of 3 to 5×10^4 per well were plated in 12-well plates for 6h, then treated with drug at indicated concentration for 24h. After treatment, cells were fixed in 75% ethanol at 4°C overnight, then the Fixed cells were stained with RNase A/PI (1:9) for 60min in dark, then analyzed by flow cytometry (488nm) using ModFit LT (VeritySoftwareHouse, USA). For apoptosis detection, all cells were collected and double-stained with Annexin V-FITC and PI using the Annexin V-FITC/PI Apoptosis Kit (MultiSciences, Hangzhou, China) according to manufacturer's instructions.

Cell death assessment was performed using SYTOX Green nucleic acid stain (KeyGEN Biotech, Nanjing, China) according to the standard protocol. Cells were plated in 12-well plates at $3\text{-}5\times10^4$ cells/well and exposed to indicated drug concentrations for 24 hours. Post-treatment, cells were gently washed with PBS and stained with SYTOX Green working solution for 10 minutes at room temperature. After three PBS washes to remove unbound dye, cell mortality was

visualized under fluorescence microscopy.

3.6 Assessment of cell migration and invasion abilities

To evaluate cell migration capacity, the wound healing scratch assay was performed firstly. Twenty-four well plates were seeded with 2×10^5 cells per well and incubated overnight. Using an aseptic p200 pipette tip, uniform linear wounds were created in the central region of each well. The wells were then replenished with serum-deprived medium containing predetermined drug concentrations. Time-lapse documentation was conducted at two time points: immediately post-wounding (0h) and after 24 hours of incubation, utilizing phase-contrast microscopy for quantitative analysis of cell migration into the denuded area.

For the invasion abilities, the Transwell assays were applied. Before seeded into the chamber, PDAC cells were planted into the 12-well plate with 5×10^4 per well and treated with drugs with indicated concentration for 24 hours. Then, cells were harvested and suspended in a 200 μL serum-free medium with about 4×10^4 cells. Subsequently, the cells were seeded into the upper chamber of transwell plates (BD Biosciences, Massachusetts, USA) precoated with or without 50 μL of Matrigel (BD Biosciences, Massachusetts, USA). At the same time, 600 μL of culture medium containing 20% FBS was added into the bottom chamber. After a 24-h incubation at 37 °C, the Transwell plates were treated with 4% paraformaldehyde for 15 min to fix the cells, followed by staining with crystal violet for another 15 min. After removing the cells from the upper chamber, invasive cells were photographed with microscope and quantified with ImageJ.

3.7 Flow cytometric measurement of cellular oxidative stress levels

PDAC cells were seeded in 12-well plates (2 to 5×10^4 cells/well) and treated with drug for 24 hours. After PBS wash, cells were stained with 10μM DCFH-DA (1:1000 dilution in serum-free medium) for 20min at 37°C. Then, cells were washed three times with serum-free medium and resuspended in 500μL serum-free medium and analyzed by flow cytometry (FITC channel). Data

were processed using FlowJo 7.6.1 (Becton Dickinson, USA).

3.8 Western blot

Protein samples were prepared by lysing cells with RIPA buffer containing both protease and phosphatase inhibitor. Protein quantification was performed using the BCA method. Subsequently, 10% SDS-polyacrylamide gel electrophoresis was employed to separate proteins and then electrotransferred onto PVDF membranes. After blocking with 5% skim milk in TBST for 60 minutes at ambient temperature, the membranes were probed with specific primary antibodies at 4°C for approximately 16 hours. Following extensive washing, the membranes were incubated with horseradish peroxidase-linked secondary antibodies for 1 hour at room temperature. Finally, target protein bands were detected through enhanced chemiluminescence using a digital imaging system.

3.9 Synergism analysis

The combination index (CI) of the combination therapy was calculated based on the drug concentration gradient and cell inhibition rate obtained from the CCK8 experiment. Cell inhibition rate=1- (OD value of the treatment group - background OD value) / (OD value of the control group - background OD value) * 100%. The specific calculation of CI index is completed in Compusyn software (Version 1.0)[40]. CI values were interpreted as follows: very strong synergistic effect (<0.1), strong synergistic effect (0.1-0.3), synergistic effect (0.3-0.7), moderate synergistic effect (0.7-0.85), mild synergistic effect (0.85-0.9), near cumulative effect (0.9-1.1), and mild antagonistic effect (1.1<).

3.10 *In vivo* xenograft experiment

For the xenograft models, after intraperitoneal anesthesia with tribromoethanol with a dosed of 150mg/kg, PANC1 and ASPC1 cells (5×10^6) were suspended in 100 μL cold PBS and subcutaneously injected into the dorsal flank of the four-week-old female BALB/c athymic nude

mice. The mice were purchased from GemPharmatech Co., Ltd. When the tumor volume reached approximately 50-100 mm^3, the mice were randomly divided into several groups followed by strict randomization and blinding rule. To minimize bias, animals were randomly assigned to experimental groups using a computer-generated randomization sequence (Microsoft Excel RAND function), ensuring equal distribution of baseline characteristics. Allocation concealment was achieved by using coded cages, with group assignments. Blinding was maintained throughout outcome assessment, where investigators performing data analysis were unaware of group allocations, which is strongly recommended by the ARRIVE 2.0 guidelines.

For monotherapy, the mice were assigned to three group (N=6 for each group for ASPC1; N=5 for each group for PANC1): control, olverembatinib (20mg/kg) and olverembatinib (40mg/kg). The mice were administered via oral gavage once every 2 days for a total of 25 days, with each mouse receiving either 100 μL of blank solvent or the corresponding dose of olverembatinib per administration. For combination therapy, the mice were scientifically and evenly divided into four groups (N=5 for each group): control group, olverembatinib (20 mg/kg) group, gemcitabine (20 mg/kg) group, and combination group (olverembatinib (20 mg/kg) + gemcitabine (20 mg/kg)). Olverembatinib was administered via oral gavage at a frequency of once every 2 days. Gemcitabine was administered via intraperitoneal injection at a frequency of twice per week. The combination group received 100 μL of the corresponding concentration of olverembatinib and gemcitabine.

The diameter and width of the tumors were measured per two days and tumor volumes were calculated as $V\ (mm^3) = 1/2 \times (\text{length} \times \text{width}^2)$. At the endpoint of the experiment, the mice were sacrificed by CO_2. According to the AVMA Guidelines for the Euthanasia of Animals (2020 Edition), the recommended method for rodents involves a gradual fill CO_2 chamber using compressed gas. The flow rate must displace 30-70% of the chamber volume per minute to minimize distress. Animals are observed continuously until respiratory arrest, after which CO_2 flow is maintained for at least one minute. The tumors were collected, weighed and photographed. The tumor growth inhibition rate (TGI, Tumor Growth Inhibition value) is

calculated using the formula: TGI= (1-RTV(experimental group)/RTV(control group))*100%, where the relative tumor volume (RTV, Relative Tumor Volume) is calculated as RTV=Ve/V0, with Ve representing the tumor volume at the experimental endpoint and V0 being the tumor volume at the start of the experiment. All animal experiments were performed under the guidance of Sun Yat-Sen University Committee for Use and Care of Laboratory Animals and were approved by animal experimentation ethics.

3.11 *In vivo* endogenous pancreatic cancer model

To address the limitation of subcutaneous models caused by the dense desmoplastic stroma, a somatic gene editing tumor models was applied to generate the endogenous pancreatic cancer model. Briefly, plasmid solution, containing one plasmid encoding the Sleeping Beauty transposase and two transposon-bearing plasmids carrying oncogenes, was in situ injected into the pancreas. Upon expression, the transposase facilitates random integration of the oncogenes into the host chromosome, enabling long-term expression and ultimately inducing malignant transformation of normal cells to form tumors[41]. In this study, four-week-old female C57BL/6J mice were purchased from GemPharmatech Co., Ltd. After intraperitoneal anesthesia with tribromoethanol with a dosed of 150mg/kg, the mouse is placed in a lateral position. Following laparotomy, the organs are exposed, and the pancreas is gently exteriorized using curved forceps. An insulin syringe is then used to aspirate the plasmid mixture (5ug pT3-AKT and pT3-MYC per mice, 1ug pCAG-SB100 per mice) and inject it into the pancreas. Finally, the organs are repositioned, the incision is sutured, and the animal is returned to a clean cage after regaining consciousness. After 2 weeks, a randomly selected mouse was euthanized to monitor pancreatic tumor formation. Drug treatment was initiated once the tumor reached 100 mm^3 in size. Group assignment was performed following the same randomization and blinding procedures described above, and the monotherapy and combination therapy regimens were identical to those used in the nude mouse model. After 7 days of treatment, the mice were euthanized by carbon dioxide asphyxiation as mentioned above. The spleen and tumor-bearing pancreas were then dissected,

photographed, weighed, and subjected to subsequent statistical analysis.

3.12 RNA-seq analysis

PANC1 and ASPC1 cells were treated with blank control, olverembatinib, gemcitabine and combination for 48h and then were collected for total RNA extraction by TRizol (ThermoFisher, USA) according to the manufacturer's protocol. Library construction and paired-end sequencing were performed on an Illumina Novaseq 6000 platform. Reads passed from the quality control were then mapped to the mice reference genome (GRCh38.p13) using HISAT2. The transcriptional abundance was generated with StringTie by comparing the results to the known transcriptome, and then calculated through Ballgown. The expression of each gene was expressed in FPKM (Fragments Per Kilobase of gene/transcript model per Million mapped fragments).

3.13 Reverse transcription qPCR

Total cellular RNA was extracted using the Albatross Rapid Cell Extraction Kit. The RNA was then reverse-transcribed into cDNA with the Transcriptor First Strand cDNA Synthesis Kit (Roche Applied Science, Branford, CT, USA). Subsequently, quantitative real-time PCR (qPCR) was performed using the FastStart SYBR Green Master (ROX) reagent (Roche Applied Science) in line with the manufacturer's protocol. The mRNA expression levels of SLC44A4 were assessed via qPCR on a Bio-Rad CFX96 system utilizing SYBR Green and gene-specific primers. GAPDH expression was used to normalize the data in triplicate samples. The primers of used were: SLC44A4 forward: GGGAAGCCAGTCAAATACGA; reverse: CCCCACCACGATGTAACCTA.

3.14 Public database

The RNA-seq dataset GSE62452 and GSE28753 related to PDAC was obtained from the Gene Expression Omnibus (GEO). Simultaneously, the RNA-seq data of TCGA-PDAC was

downloaded from TCGA database (https://portal.gdc.cancer.gov), extracting the data in Transcripts Per Million (TPM) format along with clinical information. The STRING database (https://cn.string-db.org/) was utilized to construct Protein-Protein Interaction Networks (PPIs) for target genes[42]. GEPIA (http://gepia.cancer-pku.cn/) website platform was applied to analysed the different expression of genes between normal and tumor tissue. The target gene expression (TPM) data of the 60 cancer cell lines and their IC50 values for different chemotherapeutic drugs were downloaded from CellMiner database and analyzed the correlation between them[43].

3.15 Bioinformatic analysis

The limma package of R was applied to identify the differentially expressed genes (DEGs) between different groups. The expression levels of mRNAs with |log2FoldChange| > 1 and p-value < 0.05 were used to identify the DEGs. GO (Gene Ontology) analysis, KEGG (Kyoto Encyclopedia of Genes and Genomes) pathway analysis and REACTOME pathway enrichment analysis were performed using the R package clusterProfiler. All computations were performed with the R software (version 4.1.1) system.

2.16 Ethics approval and consent to participate

For clinical research, the project was approved by the Human Research Ethics Committees of Sun Yat-sen University Cancer Center (SL-A2018-020). All participants gave informed consent to participates in this research. And all methods involving human were performed in accordance with the relevant guidelines and regulations of the Declaration of Helsinki. For animal experiment, all animal experimental procedures received approval from the SYSUCC animal experimentation ethics committee, and all methods were performed in accordance with the relevant guidelines and regulations of the Basel Declaration. and the study was reported following ARRIVE guidelines.

3.17 Statistical analysis

Statistical analysis was carried out using GraphPad Prism (Inc., San Diego, CA, USA). The data were presented as mean ± SD if without special indication. Statistical analysis between the two groups was compared using an unpaired two-tailed Student's t-test. Statistics analysis among multiple groups was compared using a one-way analysis of variance (ANOVA). The correlation analysis was performed using Pearson method. P value < 0.05 was considered a significant difference. Each experiment was conducted independently at least three times.

4. Acknowledgements and Funding

We would like to express our sincere gratitude to the patients for their contribution to this study. We also acknowledge the GEO and TCGA databases for providing high quality data. This study was supported by the National Natural Science Foundation of China (NSFC: 82172748, 82073377,82003268 and 82303807); the Natural Science Foundation of Guangdong (2021A1515012439 and 2024A1515013011); Fundamental Research Funds for the Central Universities, Sun Yat-sen University (24qnpy283); Young Talents Program of Sun Yat-sen University Cancer Center (YTP-SYSUCC-0104); Science and Technology Projects in Guangzhou (2023A04J2131)

5. Data Availability Statement

The original data of western blots has been stored in the supplementary materials. The raw RNAseq data used and analyzed during the current study are available from the corresponding author on reasonable request. The GEO datasets were obtained with accessed number GSE62452 and GSE28753. The RNA-seq data of TCGA-PDAC was downloaded from TCGA database.

6. Code Availability Statement

The code is available from the corresponding author upon reasonable request.

7. Competing interests

The authors declare no competing financial or non-financial interests.

8. Author contributions

Zengfei Xia, Qiuyun Luo, Runduan Lin and Fan Luo validated the data. Zengfei Xia and Runduan Lin performed the formal analysis. Zengfei Xia wrote the original draft. Qiuyun Luo, Yan Li and Fan Luo revised the manuscript. Qiuyun Luo developed the software tools. Runduan Lin developed the methodology. Runduan Lin, Jing Yang and Jiaxing Cao conducted the investigation. Jing Yang and Shan Shi curated the data and prepared the figures. Wenlong Guan and Miaozhen Qiu collected the clinical imaging data. Lin Zhang, Wenlong Guan and Dajun Yang conceptualized and supervised the study, managed the project and provided critical guidance and resources. All authors have read and approved the final version of the manuscript.

9. Abbreviations

TIKs, Tyrosine kinase inhibitors; FBS, Fetal bovine serum; CDX, Cell derived xenograft; PDAC, Pancreatic ductal adenocarcinoma; CML, Chronic myelogenous leukemia; PPI, Protein-protein interaction Networks; CCK8, Cell counting kit-8; WB, Western blot; GO, Gene ontology; KEGG, Kyoto Encyclopedia of Genes and Genomes; EMT, Epithelial-mesenchymal transition; ROS, Reactive oxygen species; TGI, Tumor growth inhibition value; RTV, Relative tumor volume; BP, Biological process; MF, Molecular function; CI, combination index; DEGs, different expressed genes.

References

1 Kloppel, G & Luttges J. WHO-classification 2000: exocrine pancreatic tumors. Verh Dtsch Ges Pathol, 2001; **85**: 219–228.

2 Rawla, P, Sunkara T & Gaduputi V. Epidemiology of Pancreatic Cancer: Global Trends, Etiology and Risk Factors. World J Oncol, 2019; **10**: 10–27.

3 Vaccaro, V, Sperduti I & Milella M. FOLFIRINOX versus gemcitabine for metastatic pancreatic cancer. New Engl. J. Med., 2011; **365**: 768–769; author reply 769.

4 Von Hoff, D D, Ervin T, Arena F P, Chiorean E G, Infante J, Moore M *et al.* Increased survival in pancreatic cancer with nab-paclitaxel plus gemcitabine. New Engl. J. Med., 2013; **369**: 1691–1703.

5 Goldstein, D, El-Maraghi R, Hammel P, Heinemann V, Kunzmann V, Sastre J *et al.* Updated survival from a randomized phase III trial (MPACT) of nab-paclitaxel plus gemcitabine versus gemcitabine alone for patients (pts) with metastatic adenocarcinoma of the pancreas. J. Clin. Oncol., 2014; **32**: 178.

6 Dellmann, H D. Scanning and transmission electron microscopy of the subfornical organ of the grass frog (Rana pipiens). Cell Tissue Res., 1978; **186**: 361–374.

7 Qian, Z R, Rubinson D A, Nowak J A, Morales-Oyarvide V, Dunne R F, Kozak M M *et al.* Association of Alterations in Main Driver Genes With Outcomes of Patients With Resected Pancreatic Ductal Adenocarcinoma. JAMA Oncol, 2018; **4**: e173420.

8 Aguirre, A J, Nowak J A, Camarda N D, Moffitt R A, Ghazani A A, Hazar-Rethinam M *et al.* Real-time Genomic Characterization of Advanced Pancreatic Cancer to Enable Precision Medicine. Cancer Discov., 2018; **8**: 1096–1111.

9 Hallin, J, Engstrom L D, Hargis L, Calinisan A, Aranda R, Briere D M *et al.* The KRAS(G12C) Inhibitor MRTX849 Provides Insight toward Therapeutic Susceptibility of KRAS-Mutant Cancers in Mouse Models and Patients. Cancer Discov., 2020; **10**: 54–71.

10 Hofmann, M H, Gmachl M, Ramharter J, Savarese F, Gerlach D, Marszalek J R *et al.* BI-3406, a Potent and Selective SOS1-KRAS Interaction Inhibitor, Is Effective in KRAS-Driven Cancers through Combined MEK Inhibition. Cancer Discov., 2021; **11**: 142–157.

11 Yezhelyev, M V, Koehl G, Guba M, Brabletz T, Jauch K W, Ryan A *et al.* Inhibition of SRC tyrosine kinase as treatment for human pancreatic cancer growing orthotopically in nude mice. Clin. Cancer. Res., 2004; **10**: 8028–8036.

12 Flossmann-Kast, B B, Jehle P M, Hoeflich A, Adler G & Lutz M P. Src stimulates insulin-like growth factor I (IGF-I)-dependent cell proliferation by increasing IGF-I receptor number in human pancreatic carcinoma cells. Cancer Res., 1998; **58**: 3551–3554.

13 Trevino, J G, Summy J M, Gray M J, Nilsson M B, Lesslie D P, Baker C H *et al.* Expression and activity of SRC regulate interleukin-8 expression in pancreatic adenocarcinoma cells: implications for angiogenesis. Cancer Res., 2005; **65**: 7214–7222.

14 Li, J, Hu B, Wang T, Huang W, Ma C, Zhao Q *et al.* C-Src confers resistance to mitotic stress through inhibition DMAP1/Bub3 complex formation in pancreatic cancer. Mol. Cancer, 2018; **17**: 174.

15 Su, L, Chen Y, Huang C, Wu S, Wang X, Zhao X *et al.* Targeting Src reactivates pyroptosis to reverse chemoresistance in lung and pancreatic cancer models. Sci. Transl. Med., 2023; **15**: eabl7895.

16 Duxbury, M S, Ito H, Zinner M J, Ashley S W & Whang E E. Inhibition of SRC tyrosine kinase impairs inherent and acquired gemcitabine resistance in human pancreatic adenocarcinoma cells. Clin. Cancer. Res., 2004; **10**: 2307–2318.

17 Pan, Y, Zheng M, Zhong L, Yang J, Zhou S, Qin Y *et al.* A preclinical evaluation of SKLB261, a multikinase inhibitor of EGFR/Src/VEGFR2, as a therapeutic agent against pancreatic cancer. Mol. Cancer Ther., 2015; **14**: 407–418.

18 Dhillon, S. Olverembatinib: First Approval. Drugs, 2022; **82**: 469–475.

19 Liu, X, Wang G, Yan X, Qiu H, Min P, Wu M *et al.* Preclinical development of HQP1351, a multikinase inhibitor targeting a broad spectrum of mutant KIT kinases, for the treatment of imatinib-resistant

gastrointestinal stromal tumors. Cell Biosci, 2019; **9**: 88.

20 Qiu., H, C Y, Z Z, Y Z, X W, N L *et al.* Updated efficacy results of olverembatinib (HQP1351) in patients with succinate dehydrogenase (SDH)-deficient gastrointestinal stromal tumors (GIST) and potential mechanisms of action (MOA). J Clin Oncol, 2024; **42**.

21 Mattie, M, Raitano A, Morrison K, Morrison K, An Z, Capo L *et al.* The Discovery and Preclinical Development of ASG-5ME, an Antibody-Drug Conjugate Targeting SLC44A4-Positive Epithelial Tumors Including Pancreatic and Prostate Cancer. Mol. Cancer Ther., 2016; **15**: 2679–2687.

22 Rhim, A D, Mirek E T, Aiello N M, Maitra A, Bailey J M, McAllister F *et al.* EMT and dissemination precede pancreatic tumor formation. Cell, 2012; **148**: 349–361.

23 Reynolds, A B & Roczniak-Ferguson A. Emerging roles for p120-catenin in cell adhesion and cancer. Oncogene, 2004; **23**: 7947–7956.

24 Encarnacion-Rosado, J & Kimmelman A C. Harnessing metabolic dependencies in pancreatic cancers. Nat. Rev. Gastroenterol. Hepatol., 2021; **18**: 482–492.

25 Rane, S G & Reddy E P. JAKs, STATs and Src kinases in hematopoiesis. Oncogene, 2002; **21**: 3334–3358.

26 Siesser, P M & Hanks S K. The signaling and biological implications of FAK overexpression in cancer. Clin. Cancer. Res., 2006; **12**: 3233–3237.

27 Kabil, A, Silva E & Kortenkamp A. Estrogens and genomic instability in human breast cancer cells--involvement of Src/Raf/Erk signaling in micronucleus formation by estrogenic chemicals. Carcinogenesis, 2008; **29**: 1862–1868.

28 Walz, S, Lorenzin F, Morton J, Wiese K E, von Eyss B, Herold S *et al.* Activation and repression by oncogenic MYC shape tumour-specific gene expression profiles. Nature, 2014; **511**: 483–487.

29 Saborowski, M, Saborowski A, Morris J P t, Bosbach B, Dow L E, Pelletier J *et al.* A modular and flexible ESC-based mouse model of pancreatic cancer. Genes Dev., 2014; **28**: 85–97.

30 Lin, W C, Rajbhandari N, Liu C, Sakamoto K, Zhang Q, Triplett A A *et al.* Dormant cancer cells contribute to residual disease in a model of reversible pancreatic cancer. Cancer Res., 2013; **73**: 1821–1830.

31 Farrell, A S & Sears R C. MYC degradation. Cold Spring Harb. Perspect. Med., 2014; **4**.

32 Yeh, E, Cunningham M, Arnold H, Chasse D, Monteith T, Ivaldi G *et al.* A signalling pathway controlling c-Myc degradation that impacts oncogenic transformation of human cells. Nat. Cell Biol., 2004; **6**: 308–318.

33 Sears, R, Nuckolls F, Haura E, Taya Y, Tamai K & Nevins J R. Multiple Ras-dependent phosphorylation pathways regulate Myc protein stability. Genes Dev., 2000; **14**: 2501–2514.

34 Cross, D A, Alessi D R, Cohen P, Andjelkovich M & Hemmings B A. Inhibition of glycogen synthase kinase-3 by insulin mediated by protein kinase B. Nature, 1995; **378**: 785–789.

35 Ishizawar, R C, Miyake T & Parsons S J. c-Src modulates ErbB2 and ErbB3 heterocomplex formation and function. Oncogene, 2007; **26**: 3503–3510.

36 Mori, S, Ronnstrand L, Yokote K, Engstrom A, Courtneidge S A, Claesson-Welsh L *et al.* Identification of two juxtamembrane autophosphorylation sites in the PDGF beta-receptor; involvement in the interaction with Src family tyrosine kinases. EMBO J., 1993; **12**: 2257–2264.

37 Kypta, R M, Goldberg Y, Ulug E T & Courtneidge S A. Association between the PDGF receptor and

members of the src family of tyrosine kinases. Cell, 1990; **62**: 481–492.

38 Hansen, K, Johnell M, Siegbahn A, Rorsman C, Engstrom U, Wernstedt C *et al.* Mutation of a Src phosphorylation site in the PDGF beta-receptor leads to increased PDGF-stimulated chemotaxis but decreased mitogenesis. EMBO J., 1996; **15**: 5299–5313.

39 Stark, G R & Darnell J E, Jr. The JAK-STAT pathway at twenty. Immunity, 2012; **36**: 503–514.

40 Chou, T C. Drug combination studies and their synergy quantification using the Chou-Talalay method. Cancer Res., 2010; **70**: 440–446.

41 Niu, Y, Ding C, Wang Q, Yin J, Li L, Liu W *et al.* TRIM6 ablation reverses ICB resistance in MSS gastric cancer by unleashing cGAS-STING-dependent antitumor immunity. #N/A, 2025; **44**: 242.

42 Szklarczyk, D, Gable A L, Lyon D, Junge A, Wyder S, Huerta-Cepas J *et al.* STRING v11: protein-protein association networks with increased coverage, supporting functional discovery in genome-wide experimental datasets. Nucleic Acids Res., 2019; **47**: D607–D613.

43 Luna, A, Elloumi F, Varma S, Wang Y, Rajapakse V N, Aladjem M I *et al.* CellMiner Cross-Database (CellMinerCDB) version 1.2: Exploration of patient-derived cancer cell line pharmacogenomics. Nucleic Acids Res., 2021; **49**: D1083–D1093.

Figure Legends

Figure 1. Olverembatinib inhibits the cell vitality and proliferation of PDAC cells. (A) The 72 hours IC50 values of olverembatinib in different cancer cell lines (Unit: uM/mL). (B) Olverembatinib inhibited the cell viability of pancreatic cancer cell lines in concentration and time dependent manner. (C) Representative cell morphology images of pancreatic cancer cells treated with different concentration of olverembatinib. (D) The plate colony formation showed the inhibition effect of olverembatinib on the proliferation of pancreatic cancer cells in a

concentration dependent manner. (E-F) EdU immunofluorescence staining showed significant reduction of the proportion of pancreatic cancer cells in proliferative state after the treatment with olverembatinib for 24 hours. (Green fluorescence refers to EdU staining, which representing cells in DNA replication, and blue refers to the cell nuclei). Results are shown as mean ± SEM. * $P < 0.05$, ** $P < 0.01$, ***$P < 0.001$.

Figure 2. Olverembatinib blocks pancreatic cancer cells in G1 phase of cell cycle and induces apoptosis in pancreatic cancer cells. (A-B) The induction of G1 cell cycle arrest in pancreatic cancer cells treated with olverembatinib for 24 hours. (C-D) After the treatment with olverembatinib, the expression changes of cyclinD1 and CDK4 proteins in pancreatic cancer cells. (E-F) Flow cytometry assay showed the induction of apoptosis in pancreatic cancer cells treated with olverembatinib. (G-H) The green cyanine SYTOX staining showed the dead pancreatic cancer cells and the changes of their proportion in the total cells under the olverembatinib treatment. (Green fluorescence is the SYTOX dye, representing the dead cells). Results are shown as mean ± SEM. * $P < 0.05$, ** $P < 0.01$, ***$P < 0.001$.

Figure 3. Olverembatinib inhibits the migration and invasion and upregulates the intracellular ROS level of pancreatic cancer cells. (A-B) Wound healing assay was performed to evaluate the inhibitory effect of olverembatinib on the migration capacity of pancreatic cancer cells. (C-E) The transwell assays showed the inhibitory effect of olverembatinib on the migration and invasion ability of pancreatic cancer cells. (F) WB results showed the expression regulation of EMT-regulated proteins by olverembatinib. (G) The flow cytometry detection of DCFH-DA in pancreatic cancer cells after the olverembatinib treatment. (H) olverembatinib upregulated the level of intracellular ROS level in pancreatic cancer cells. (I) The WB results showed the expression regulation of NRF2 by olverembatinib in pancreatic cancer cells. Results are shown as mean ± SEM. * $P < 0.05$, ** $P < 0.01$, ***$P < 0.001$.

Figure 4. Olverembatinib inhibits the SRC/AKT/MYC signaling in pancreatic cancer cells. (A) The inhibition rate of various kinases by olverembatinib at 10 nM (Offered by Ascentage Pharma). (B) The BP and MF enrichment analysis of the targeted genes. (C) The PPI interaction network of the targets of olverembatinib constructed by STRING database. (D-E) The differential analysis of gene expression of SRC and MYC between tumor and adjacent normal tissues in the TCGA-PDAC cohort. (F) The protein expression and phosphorylation level change of SRC in pancreatic cancer cells treated with indicated olverembatinib. (G) The KEGG and REACTOME pathway enrichment analysis of the targeted genes. (H-I) Olverembatinib had no effect on the expression and phosphorylation levels of ERK1/2 and STAT3 in pancreatic cancer cells. (J) The inhibitory effect of olverembatinib on the protein expression and phosphorylation levels of AKT and cMYC in pancreatic cancer cells. * $P < 0.05$, ** $P < 0.01$, ***$P < 0.001$.

Figure 5. AKT activation rescue the anti-tumor efficiency of olverembatinib. (A) The plate colony formation showed the inhibition effect of olverembatinib on the proliferation was rescued by AKT activator (SC79). (B) AKT activator decreases the apoptosis induced by olverembatinib in pancreatic cancer cells. (C-D) The transwell assays and wound healing assay showed the inhibitory effect of olverembatinib on the migration and invasion were rescued by AKT activator. (SC79, 10μg/mL for PANC1, 15μg/mL for ASPC1, 15μg/mL for BXPC3). * $P < 0.05$, ** $P < 0.01$, ***$P < 0.001$.

Figure 6. Transcriptome changes in PDAC cells after olverembatinib treatment. (A) The PCA analysis for the ASPC1 and PANC1 treated with control, olverembatinib, Gemcitabine and combination. (B) The volcano plot showed the DEGs for PANC1 and ASPC1 between olverembatinib treatment and control. (C-D) The GO and KEGG analysis for the DEGs of PANC1 and ASPC1. E. The GSEA pathway enrichment for the MF and KEGG pathways activated in olverembatinib treatment group for PANC1 and ASPC1.

Figure 7. Olverembatinib inhibits PDAC tumor growth in vivo. (A-B, D-E) The tumor size of xenograft tumor samples in ASPC1 (N=6 for each group) and PANC1 (N=5 for each group) animal models after treatment with different doses of olverembatinib. (C, F) The end-point tumor weight of xenograft tumor samples in ASPC1 and PANC1 animal models after treatment with different doses of olverembatinib. (G) The TGI index of 20mg/kg and 40 mg/kg group with bank control as reference in ASPC1 and PANC1. (H) The body weight changes in different group in ASPC1 and PANC1 mice model. (I) The changes in the phosphorylation of SRC, AKT and cMYC, the expression levels of EMT markers by WB of tumor proteins from the ASPC1 and PANC1 animal models treated with olverembatinib or not. * $P < 0.05$, ** $P < 0.01$, ***$P < 0.001$.

Figure 8. Olverembatinib combined with gemcitabine synergistic inhibits PDAC tumor growth. (A) The inhibition of cell viability of PANC1, ASPC and BXPC3 after treated with different concentration of gemcitabine for 72 hours. (B) The inhibition of cell viability of pancreatic cancer cells after treated with single agent or the combination for 72 hours. (C) The IC50 of different treatment group in the three pancreatic cancer cells (PANC1, ASPC1 and BXPC3). (D) The CI index in different cells were calculated by using Compusyn software. (E-F) The death induction in pancreatic cancer cells treated with olverembatinib, gemcitabine and in combination (Green fluorescence is the SYTOX dye, representing the dead cells). (G) The arrest of the cell cycle in pancreatic cancer cells treated with olverembatinib, gemcitabine and in combination. (H) The corresponding statistical chart for the proportion of different phase in cell cycle. * $P<0.05$, ** $P<0.01$, *** $P<0.001$.

Figure 9. Transcriptome changes in PDAC cells after olverembatinib combined with gemcitabine treatment. (A) The scatter plots showed the correlation between the gene expression of SRC, AKT, and MYC and the IC50 of gemcitabine, paclitaxel, irinotecan, 5-FU, and oxaliplatin. The X-axis represents the gene expression level (log2 (FPMK+1)), and the Y-

axis represents the Z score of IC50. Spearman method was used for the correlation analysis. (B-C) The volcano plot showed the DEGs for PANC1 and ASPC1 between combination and gemcitabine monotherapy, gemcitabine monotherapy and blank control. (D-E) The REACTOME analysis for the DEGs of PANC1 and ASPC1 in different comparison. (F-G) The REACTOME analysis for the upregulated genes (Red) and downregulated genes (Blue) of PANC1 and ASPC1 in different comparison. (H-K) The GSEA pathway enrichment showed the interferon gamma pathway change in PANC1 and ASPC1 when treated with different therapeutic regimen.

Figure 10. Olverembatinib combined with gemcitabine synergistic inhibits PDAC tumor growth in vivo. (A, D) At the end point of the experiment, the tumor gross specimens in different treatment groups of mice (N=5 for each group) were collected. (B-C, E-F) The diagram showed the tumor volume changes during the administration and the tumor weight at the end point in different treatment groups of mice. (G) The TGI index of different group with bank control as reference in ASPC1 and PANC1. (H-I) The body weight changes in different group in ASPC1 and PANC1 mice model. (J) The changes in the phosphorylation of SRC, and the interferon-gamma signaling pathway (JAK1-STAT1) activation by WB of tumor proteins from the ASPC1 and PANC1 animal models treated with blank control, olverembatinib monotherapy, gemcitabine monotherapy or combination. * $P < 0.05$, ** $P < 0.01$, ***$P < 0.001$.

Figure 11. The anti-tumor efficiency of Olverembatinib monotherapy or combined with gemcitabine in endogenous pancreatic cancer model. (A) The schematic diagram illustrates the generation of endogenous pancreatic cancer model via orthotopic pancreatic injection of AKT/MYC plasmids (N=5 for each group). (B) Mice in the single-agent group were treated according to the dosing regimen shown. (C-D) The olverembatinib monotherapy markedly reduced the relative weight of tumor-bearing pancreas. (E) The body weight change of mice during the olverembatinib monotherapy. (F) The changes in the phosphorylation of SRC, AKT and MYC by WB of tumor proteins from the endogenous pancreatic cancer model treated with

olverembatinib or not. (G) Administration schedule for the combination treatment of olverembatinib and gemcitabine. (H-I) The tumor volume changes during the administration and the tumor weight at the end point in different treatment groups of mice. (J) The changes in the phosphorylation of SRC, and the interferon-gamma signaling pathway (JAK1-STAT1) activation by WB of tumor proteins from the endogenous pancreatic cancer model in different group. * $P < 0.05$, ** $P < 0.01$, ***$P < 0.001$.

Figure 12. Olverembatinib effectively inhibited tumor size in PDAC patient

(A) A representative case of PDAC patient treated with olverembatinib. Flow chart showing the treatment options for the patient. (B) The base information of the PDAC patient. (C) CT Imaging showing the response of this PDAC patient to olverembatinib treatment.

Figure 13. Graphic abstract of SRC/AKT/MYC inhibition induced by olverembatinib and the synergistic anticancer effect of combination with gemcitabine in PDAC cells.

Fig.1

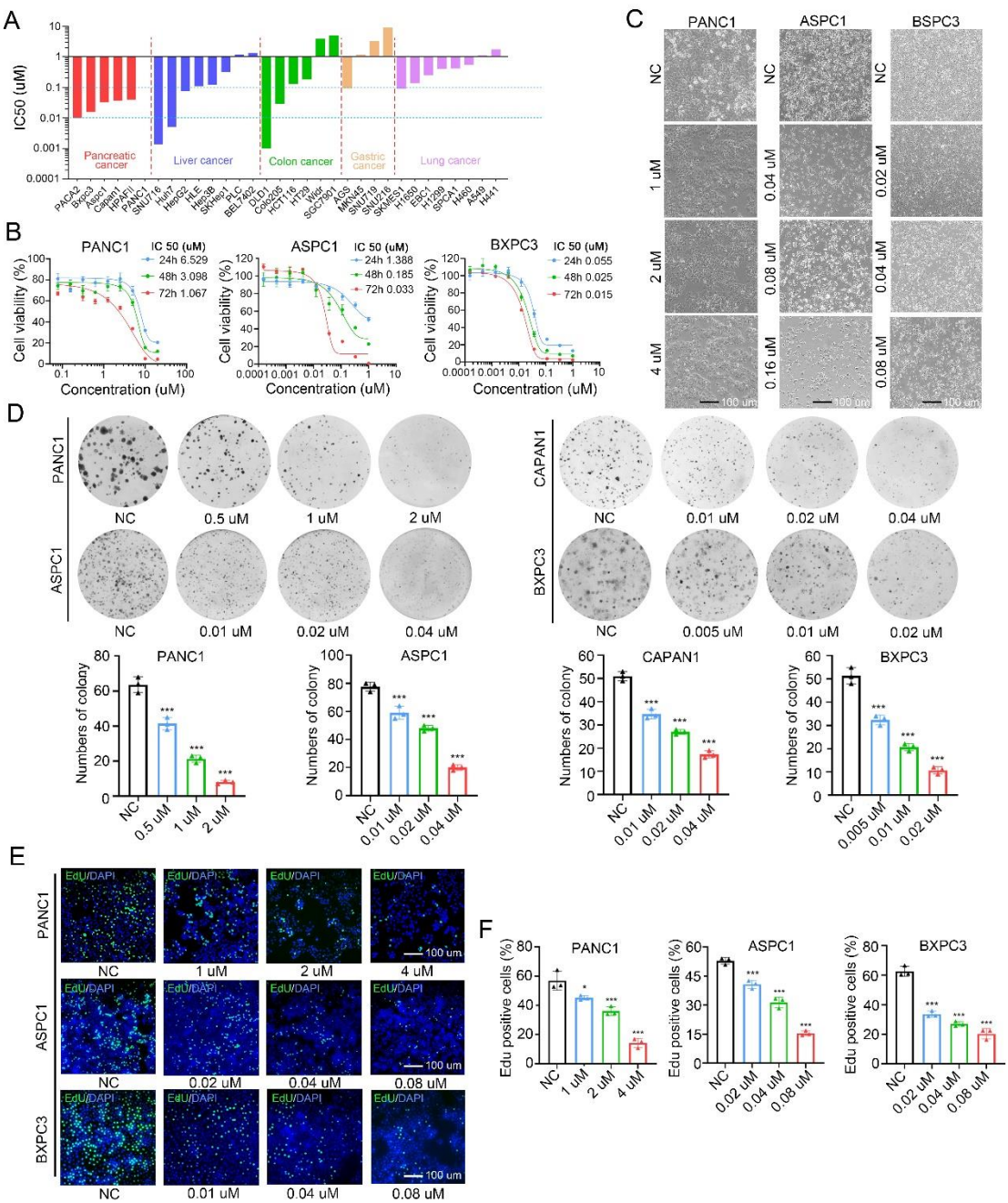
A
IC50 (uM)
Pancreatic cancer
Liver cancer
Colon cancer
Gastric cancer
Lung cancer
B
PANC1
ASPC1
BXPC3
IC 50 (uM)
24h 6.529
48h 3.098
72h 1.067
24h 1.388
48h 0.185
72h 0.033
24h 0.055
48h 0.025
72h 0.015
Cell viability (%)
Concentration (uM)
C
PANC1
ASPC1
BSPC3
NC
1 uM
2 uM
4 uM
0.04 uM
0.08 uM
0.16 uM
0.02 uM
100 um
D
PANC1
ASPC1
CAPAN1
BXPC3
NC
0.5 uM
1 uM
2 uM
0.01 uM
0.02 uM
0.04 uM
0.005 uM
Numbers of colony
E
EdU/DAPI
100 um
F
Edu positive cells (%)

Fig.2

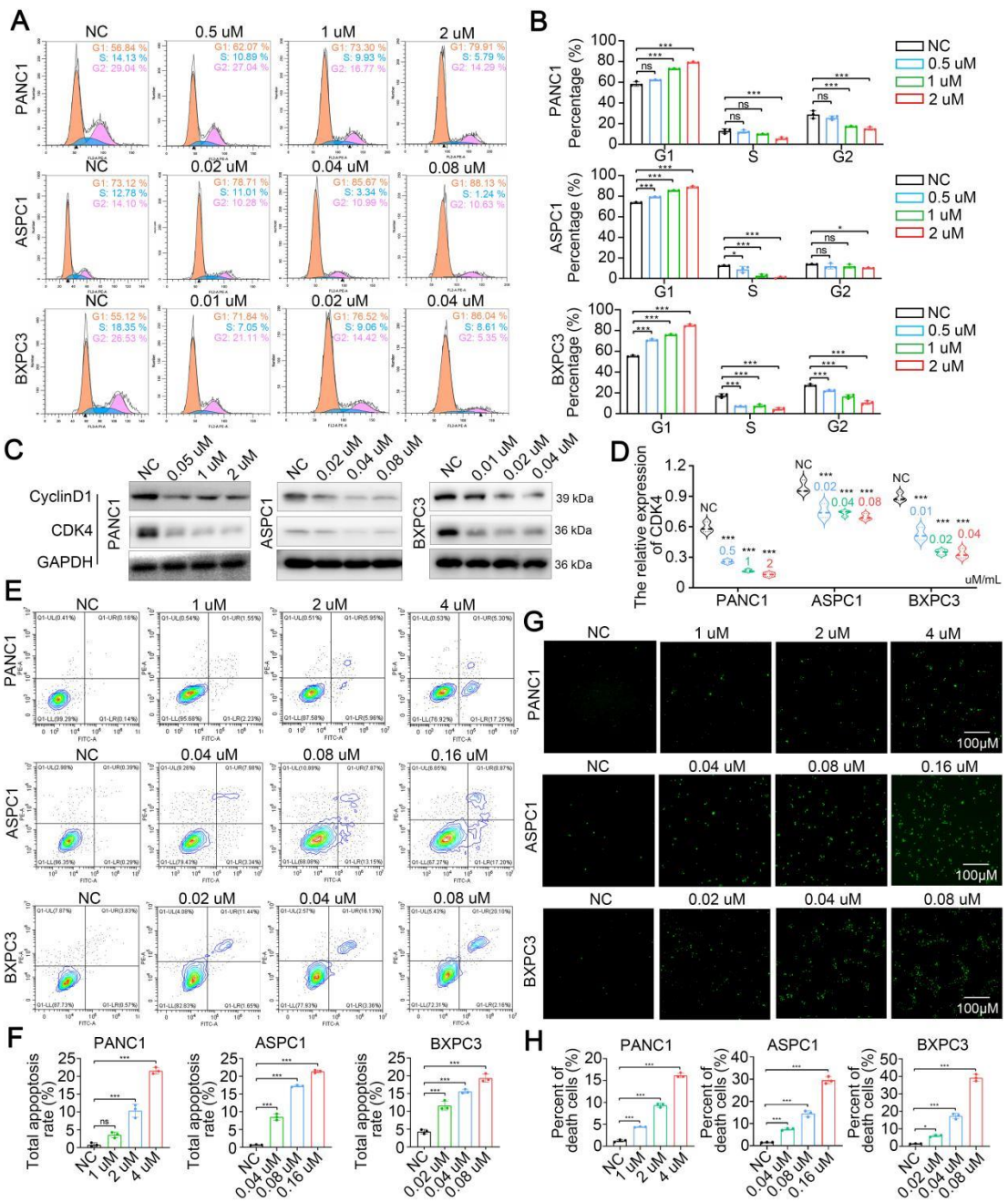
A
NC
0.5 uM
1 uM
2 uM
PANC1
G1: 56.84 %
S: 14.13 %
G2: 29.04 %
G1: 62.07 %
S: 10.89 %
G2: 27.04 %
G1: 73.30 %
S: 9.93 %
G2: 16.77 %
G1: 79.91 %
S: 5.79 %
G2: 14.29 %
NC
0.02 uM
0.04 uM
0.08 uM
ASPC1
G1: 73.12 %
S: 12.78 %
G2: 14.10 %
G1: 78.71 %
S: 11.01 %
G2: 10.28 %
G1: 85.67 %
S: 3.34 %
G2: 10.99 %
G1: 88.13 %
S: 1.24 %
G2: 10.63 %
NC
0.01 uM
0.02 uM
0.04 uM
BXPC3
G1: 55.12 %
S: 18.35 %
G2: 26.53 %
G1: 71.84 %
S: 7.05 %
G2: 21.11 %
G1: 76.52 %
S: 9.06 %
G2: 14.42 %
G1: 86.04 %
S: 8.61 %
G2: 5.35 %
B
PANC1 Percentage (%)
ASPC1 Percentage (%)
BXPC3 Percentage (%)
G1
S
G2
NC
0.5 uM
1 uM
2 uM
C
CyclinD1
CDK4
GAPDH
PANC1
ASPC1
BXPC3
39 kDa
36 kDa
36 kDa
D
The relative expression of CDK4
PANC1
ASPC1
BXPC3
uM/mL
E
NC
1 uM
2 uM
4 uM
0.04 uM
0.08 uM
0.16 uM
0.02 uM
F
PANC1
ASPC1
BXPC3
Total apoptosis rate (%)
G
100μM
H
Percent of death cells (%)

Fig.3

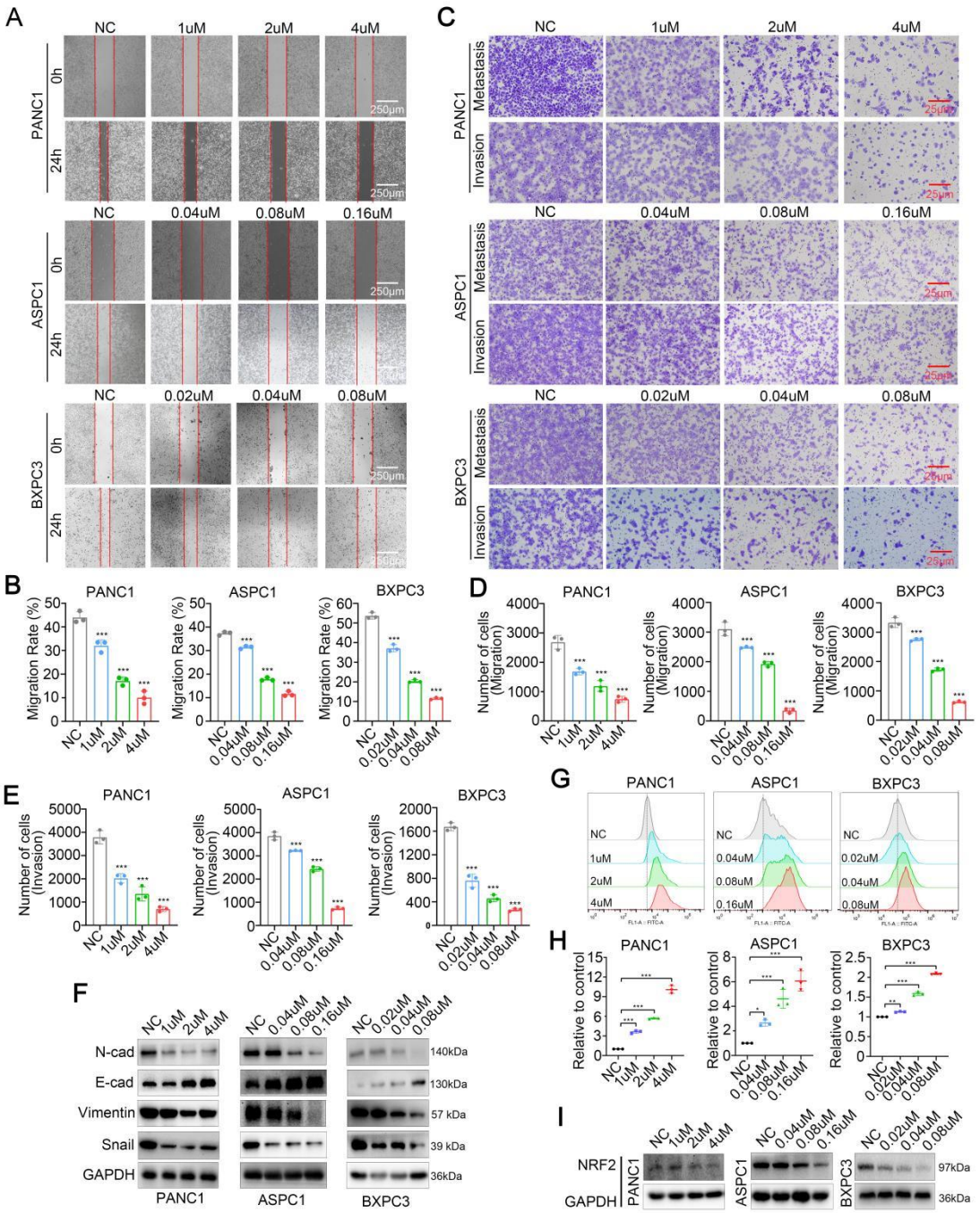
A
NC
1uM
2uM
4uM
PANC1
0h
24h
250μm
NC
0.04uM
0.08uM
0.16uM
ASPC1
NC
0.02uM
0.04uM
0.08uM
BXPC3
C
Metastasis
Invasion
25μm
B
Migration Rate (%)
D
Number of cells (Migration)
E
Number of cells (Invasion)
F
N-cad
E-cad
Vimentin
Snail
GAPDH
140kDa
130kDa
57 kDa
39 kDa
36kDa
G
H
Relative to control
I
NRF2
97kDa

Fig.4

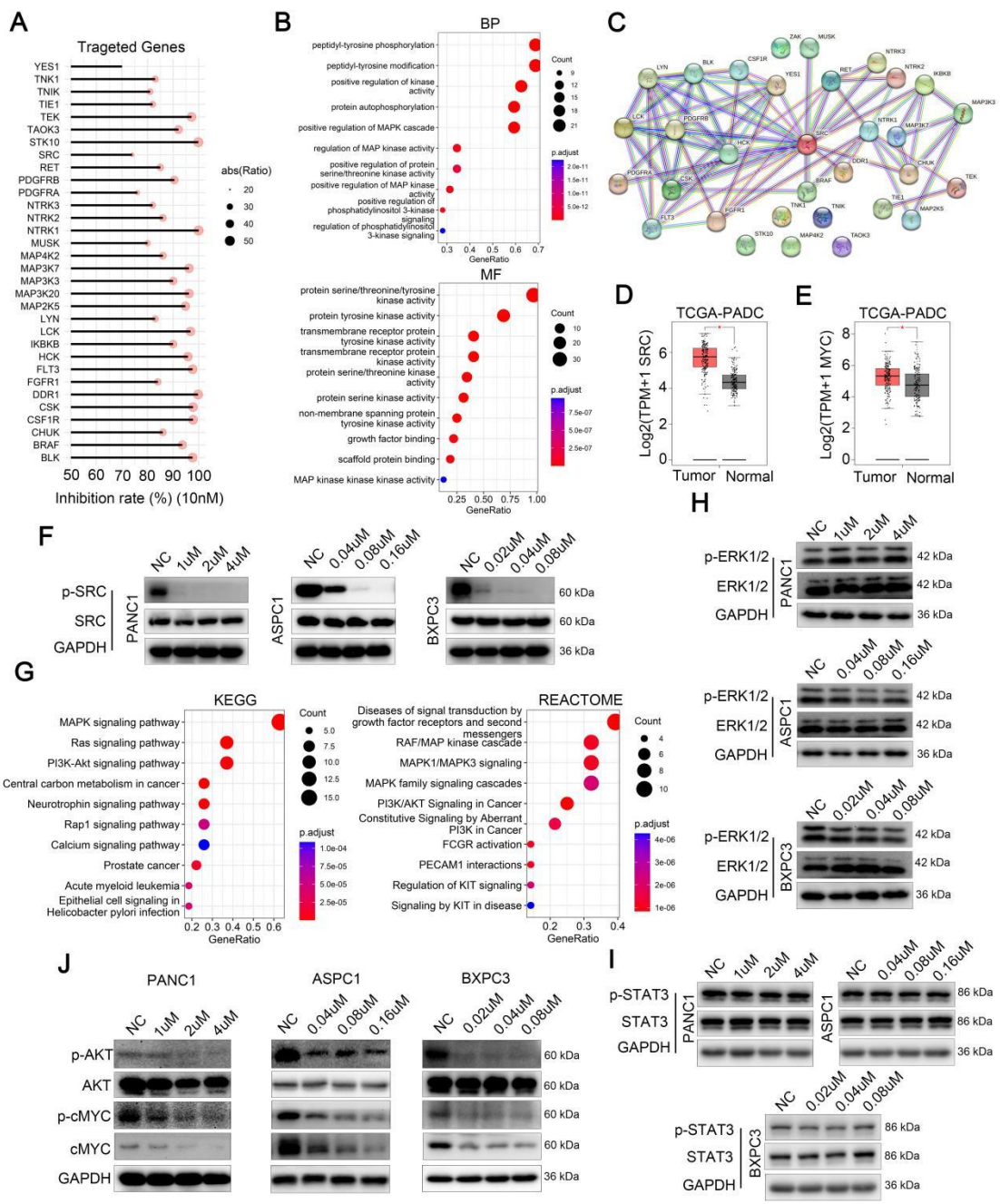
A
Trageted Genes
YES1
TNK1
TNIK
TIE1
TEK
TAOK3
STK10
SRC
RET
PDGFRB
PDGFRA
NTRK3
NTRK2
NTRK1
MUSK
MAP4K2
MAP3K7
MAP3K3
MAP3K20
MAP2K5
LYN
LCK
IKBKB
HCK
FLT3
FGFR1
DDR1
CSK
CSF1R
CHUK
BRAF
BLK
abs(Ratio)
20
30
40
50
50 60 70 80 90 100
Inhibition rate (%) (10nM)
B
BP
peptidyl-tyrosine phosphorylation
peptidyl-tyrosine modification
positive regulation of kinase activity
protein autophosphorylation
positive regulation of MAPK cascade
regulation of MAP kinase activity
positive regulation of protein serine/threonine kinase activity
positive regulation of MAP kinase activity
positive regulation of phosphatidylinositol 3-kinase signaling
regulation of phosphatidylinositol 3-kinase signaling
Count
p.adjust
GeneRatio
MF
protein serine/threonine/tyrosine kinase activity
protein tyrosine kinase activity
transmembrane receptor protein tyrosine kinase activity
transmembrane receptor protein kinase activity
protein serine/threonine kinase activity
protein serine kinase activity
non-membrane spanning protein tyrosine kinase activity
growth factor binding
scaffold protein binding
MAP kinase kinase kinase activity
C
D
TCGA-PADC
Log2(TPM+1 SRC)
Tumor
Normal
E
TCGA-PADC
Log2(TPM+1 MYC)
Tumor
Normal
F
NC
1uM
2uM
4uM
p-SRC
SRC
GAPDH
PANC1
0.04uM
0.08uM
0.16uM
ASPC1
0.02uM
0.04uM
0.08uM
BXPC3
60 kDa
36 kDa
G
KEGG
MAPK signaling pathway
Ras signaling pathway
PI3K-Akt signaling pathway
Central carbon metabolism in cancer
Neurotrophin signaling pathway
Rap1 signaling pathway
Calcium signaling pathway
Prostate cancer
Acute myeloid leukemia
Epithelial cell signaling in Helicobacter pylori infection
Count
p.adjust
GeneRatio
REACTOME
Diseases of signal transduction by growth factor receptors and second messengers
RAF/MAP kinase cascade
MAPK1/MAPK3 signaling
MAPK family signaling cascades
PI3K/AKT Signaling in Cancer
Constitutive Signaling by Aberrant PI3K in Cancer
FCGR activation
PECAM1 interactions
Regulation of KIT signaling
Signaling by KIT in disease
H
p-ERK1/2
ERK1/2
GAPDH
42 kDa
36 kDa
I
p-STAT3
STAT3
GAPDH
86 kDa
J
PANC1
ASPC1
BXPC3
p-AKT
AKT
p-cMYC
cMYC
60 kDa

Fig.5

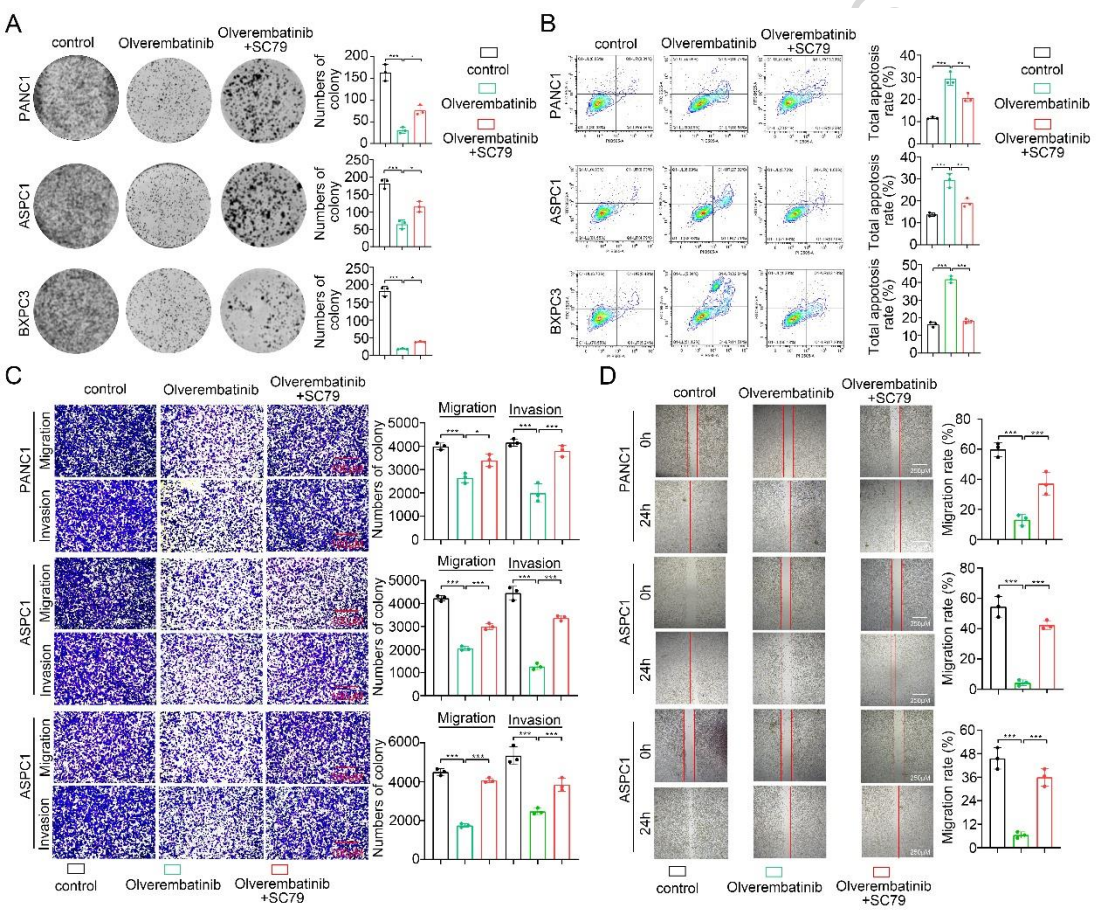
A
control
Olverembatinib
Olverembatinib +SC79
PANC1
ASPC1
BXPC3
Numbers of colony
B
Total apoptosis rate (%)
C
Migration
Invasion
D
0h
24h
Migration rate (%)

Fig.6

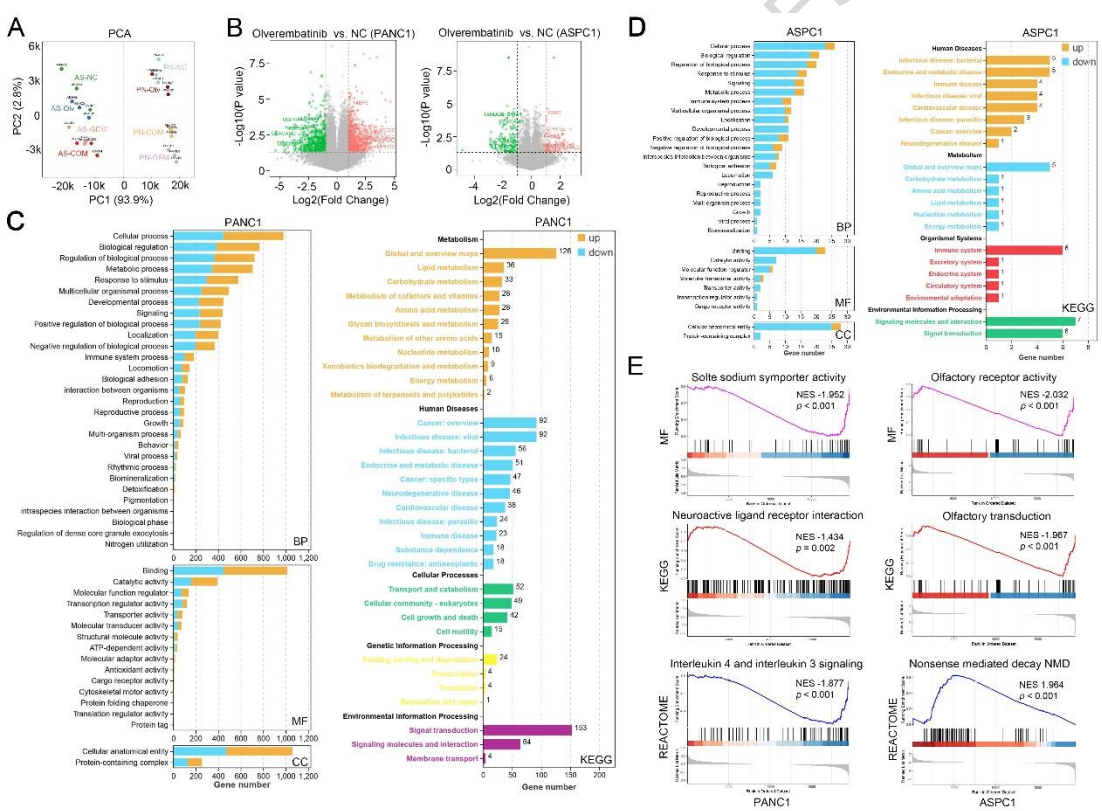

Fig.7

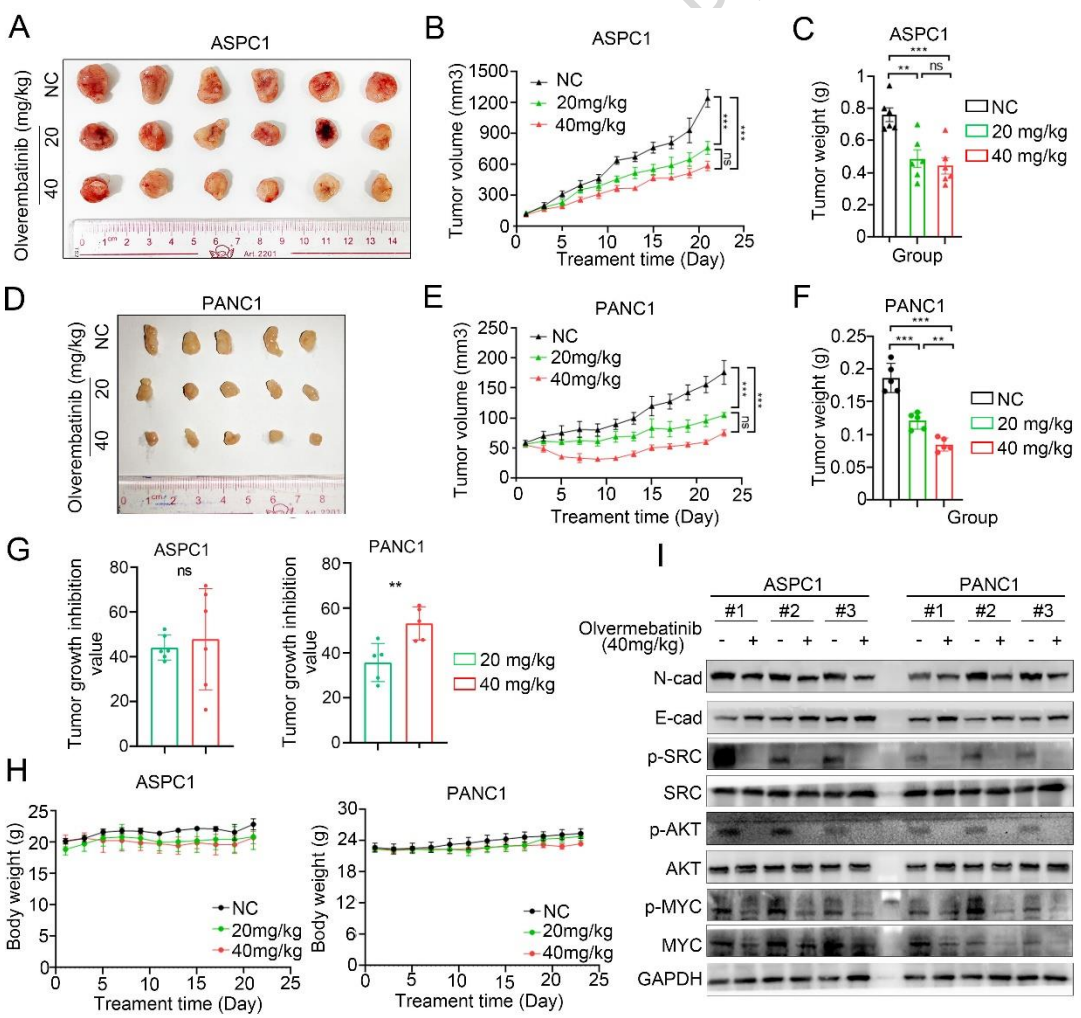
A
ASPC1
Olverembatinib (mg/kg)
NC
20
40
B
ASPC1
Tumor volume (mm3)
NC
20mg/kg
40mg/kg
Treament time (Day)
C
ASPC1
Tumor weight (g)
NC
20 mg/kg
40 mg/kg
Group
D
PANC1
Olverembatinib (mg/kg)
E
PANC1
Tumor volume (mm3)
F
PANC1
Tumor weight (g)
G
ASPC1
PANC1
Tumor growth inhibition value
20 mg/kg
40 mg/kg
H
ASPC1
PANC1
Body weight (g)
Treament time (Day)
I
ASPC1
PANC1
Olvermebatinib (40mg/kg)
N-cad
E-cad
p-SRC
SRC
p-AKT
AKT
p-MYC
MYC
GAPDH

Fig.8

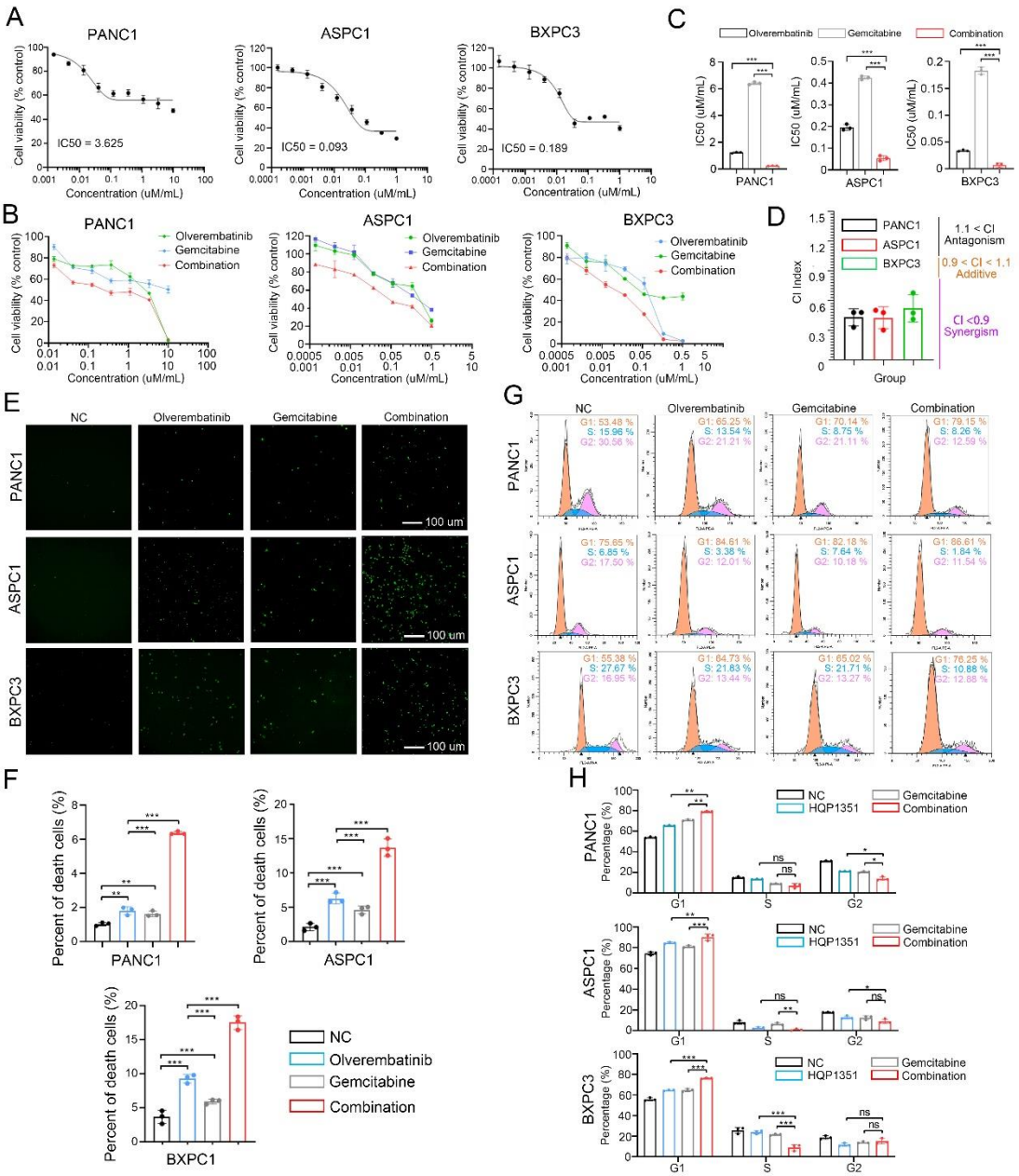
A
PANC1
ASPC1
BXPC3
Cell viability (% control)
IC50 = 3.625
IC50 = 0.093
IC50 = 0.189
Concentration (uM/mL)
B
Olverembatinib
Gemcitabine
Combination
C
Olverembatinib
Gemcitabine
Combination
IC50 (uM/mL)
D
CI index
Group
1.1 < CI Antagonism
0.9 < CI < 1.1 Additive
CI <0.9 Synergism
E
NC
Olverembatinib
Gemcitabine
Combination
100 um
F
Percent of death cells (%)
G
G1: 53.48 %
S: 15.96 %
G2: 30.56 %
G1: 65.25 %
S: 13.54 %
G2: 21.21 %
G1: 70.14 %
S: 8.75 %
G2: 21.11 %
G1: 79.15 %
S: 8.26 %
G2: 12.59 %
G1: 75.65 %
S: 6.85 %
G2: 17.50 %
G1: 84.61 %
S: 3.38 %
G2: 12.01 %
G1: 82.18 %
S: 7.64 %
G2: 10.18 %
G1: 86.61 %
S: 1.84 %
G2: 11.54 %
G1: 55.38 %
S: 27.67 %
G2: 16.95 %
G1: 64.73 %
S: 21.83 %
G2: 13.44 %
G1: 65.02 %
S: 21.71 %
G2: 13.27 %
G1: 76.25 %
S: 10.88 %
G2: 12.88 %
H
NC
HQP1351
Gemcitabine
Combination
Percentage (%)
G1
S
G2
ns

Fig.9

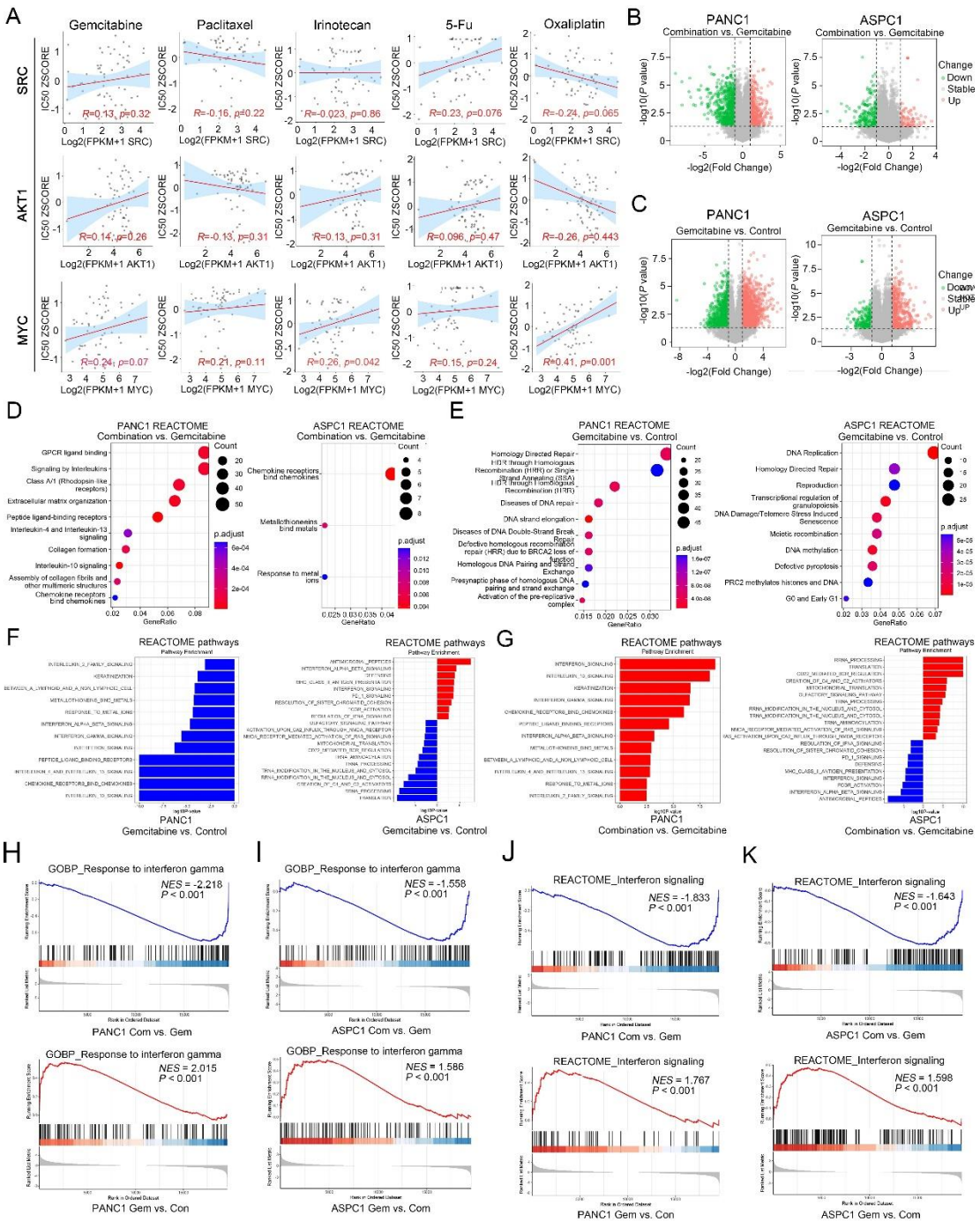
A
Gemcitabine
Paclitaxel
Irinotecan
5-Fu
Oxaliplatin
SRC
AKT1
MYC
IC50 ZSCORE
Log2(FPKM+1 SRC)
Log2(FPKM+1 AKT1)
Log2(FPKM+1 MYC)
R=0.13, p=0.32
R=-0.16, p=0.22
R=-0.023, p=0.86
R=0.23, p=0.076
R=-0.24, p=0.065
R=0.14, p=0.26
R=-0.13, p=0.31
R=0.13, p=0.31
R=0.096, p=0.47
R=-0.26, p=0.443
R=0.24, p=0.07
R=0.21, p=0.11
R=0.26, p=0.042
R=0.15, p=0.24
R=0.41, p=0.001
B
PANC1
Combination vs. Gemcitabine
ASPC1
Combination vs. Gemcitabine
-log10(P value)
-log2(Fold Change)
Change
Down
Stable
Up
C
PANC1
Gemcitabine vs. Control
ASPC1
Gemcitabine vs. Control
D
PANC1 REACTOME
Combination vs. Gemcitabine
ASPC1 REACTOME
Combination vs. Gemcitabine
GPCR ligand binding
Signaling by Interleukins
Class A/1 (Rhodopsin-like receptors)
Extracellular matrix organization
Peptide ligand-binding receptors
Interleukin-4 and Interleukin-13 signaling
Collagen formation
Interleukin-10 signaling
Assembly of collagen fibrils and other multimeric structures
Chemokine receptors bind chemokines
Metallothioneins bind metals
Response to metal ions
Count
p.adjust
GeneRatio
E
PANC1 REACTOME
Gemcitabine vs. Control
ASPC1 REACTOME
Gemcitabine vs. Control
Homology Directed Repair
HDR through Homologous Recombination (HRR) or Single-Strand Annealing (SSA)
HDR through Homologous Recombination (HRR)
Diseases of DNA repair
DNA strand elongation
Diseases of DNA Double-Strand Break Repair
Defective homologous recombination repair (HRR) due to BRCA2 loss of function
Homologous DNA Pairing and Strand Exchange
Presynaptic phase of homologous DNA pairing and strand exchange
Activation of the pre-replicative complex
DNA Replication
Homology Directed Repair
Reproduction
Transcriptional regulation of granulopoiesis
DNA Damage/Telomere Stress Induced Senescence
Meiotic recombination
DNA methylation
Defective pyroptosis
PRC2 methylates histones and DNA
G0 and Early G1
F
REACTOME pathways
Pathway Enrichment
PANC1
Gemcitabine vs. Control
ASPC1
Gemcitabine vs. Control
G
REACTOME pathways
Pathway Enrichment
PANC1
Combination vs. Gemcitabine
ASPC1
Combination vs. Gemcitabine
H
GOBP_Response to interferon gamma
NES = -2.218
P < 0.001
PANC1 Com vs. Gem
GOBP_Response to interferon gamma
NES = 2.015
P < 0.001
PANC1 Gem vs. Con
I
GOBP_Response to interferon gamma
NES = -1.558
P < 0.001
ASPC1 Com vs. Gem
GOBP_Response to interferon gamma
NES = 1.586
P < 0.001
ASPC1 Gem vs. Com
J
REACTOME_Interferon signaling
NES = -1.833
P < 0.001
PANC1 Com vs. Gem
REACTOME_Interferon signaling
NES = 1.767
P < 0.001
PANC1 Gem vs. Con
K
REACTOME_Interferon signaling
NES = -1.643
P < 0.001
ASPC1 Com vs. Gem
REACTOME_Interferon signaling
NES = 1.598
P < 0.001
ASPC1 Gem vs. Com

Fig.10

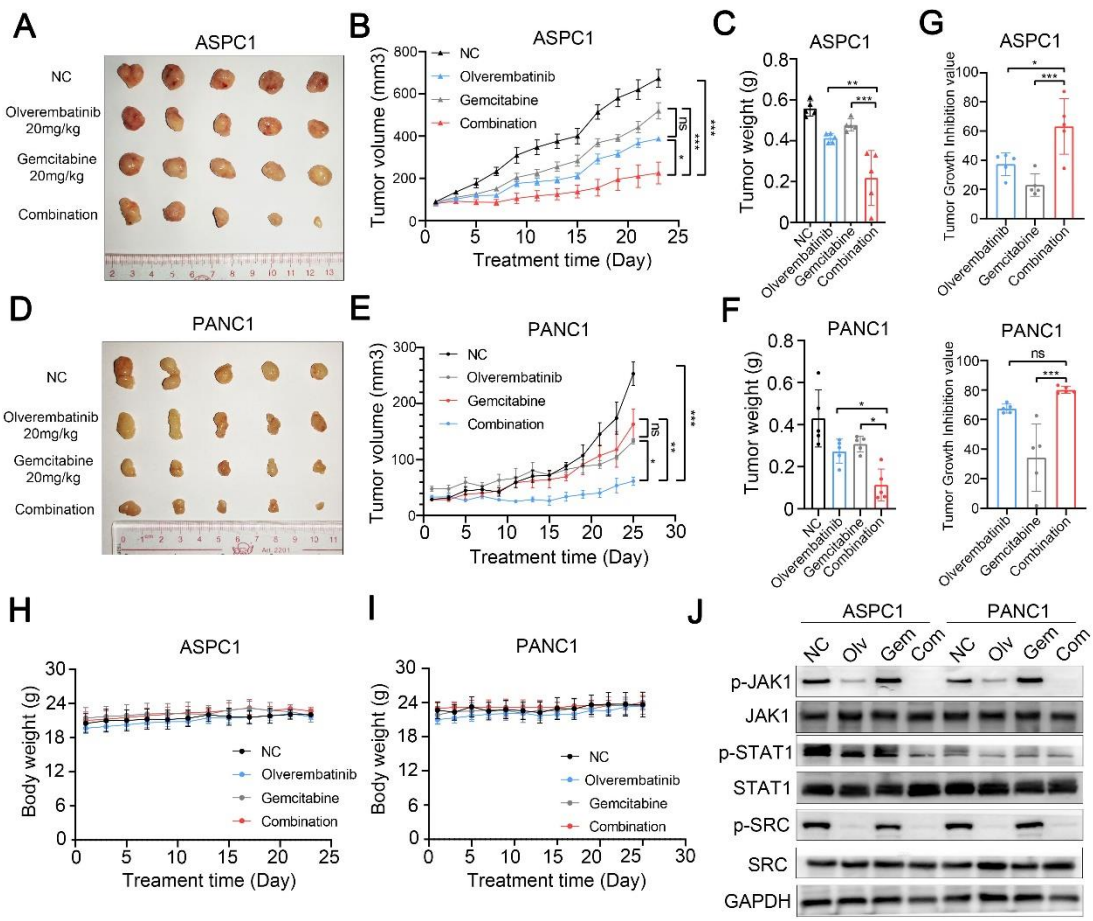
A
ASPC1
NC
Olverembatinib 20mg/kg
Gemcitabine 20mg/kg
Combination
B
ASPC1
Tumor volume (mm3)
Treatment time (Day)
NC
Olverembatinib
Gemcitabine
Combination
C
ASPC1
Tumor weight (g)
G
ASPC1
Tumor Growth Inhibition value
D
PANC1
E
PANC1
F
PANC1
ns
H
ASPC1
Body weight (g)
Treament time (Day)
I
PANC1
J
ASPC1
PANC1
NC
Olv
Gem
Com
p-JAK1
JAK1
p-STAT1
STAT1
p-SRC
SRC
GAPDH

Fig.11

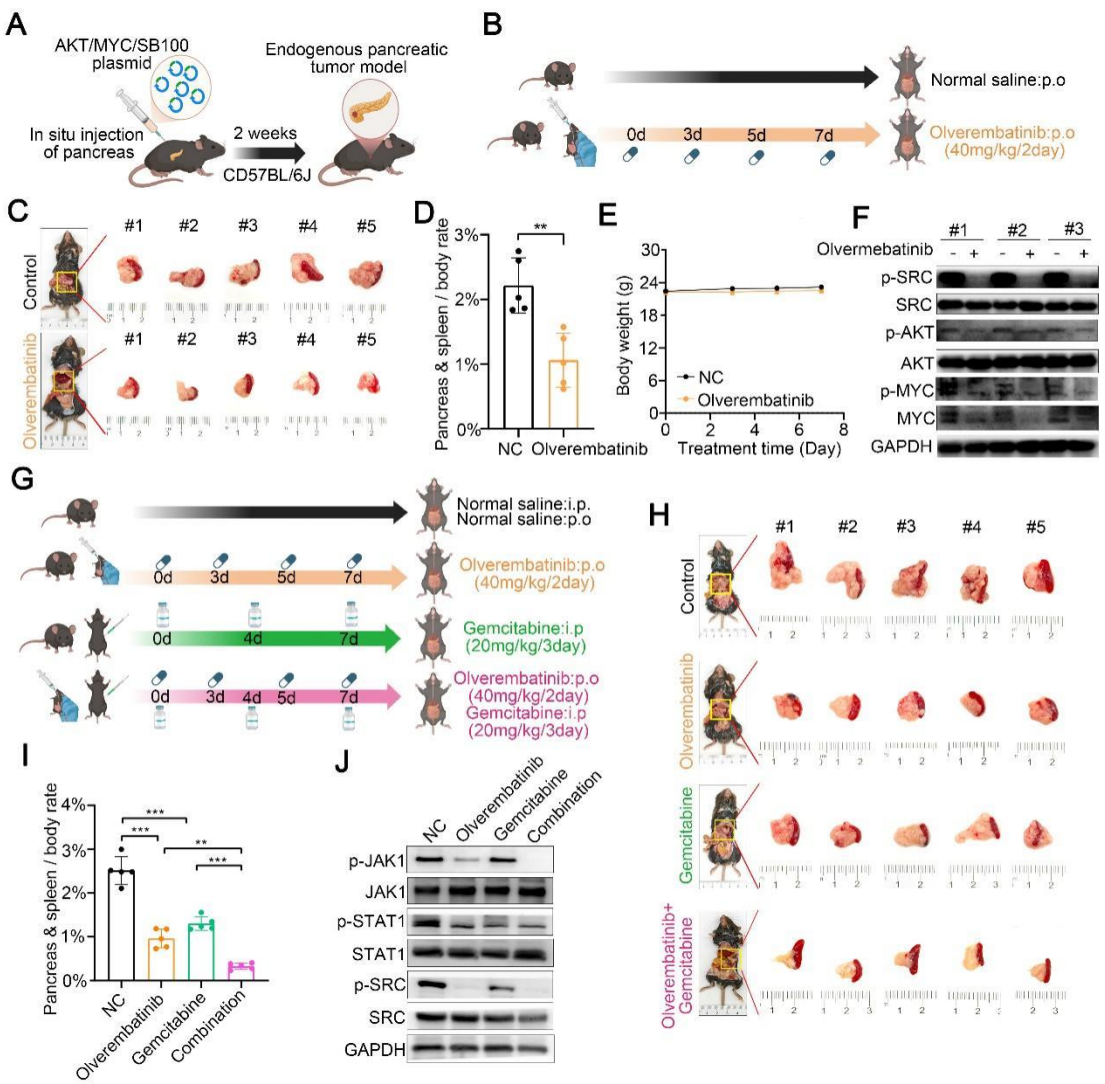
A
AKT/MYC/SB100 plasmid
In situ injection of pancreas
2 weeks
CD57BL/6J
Endogenous pancreatic tumor model
B
Normal saline:p.o
0d 3d 5d 7d
Olverembatinib:p.o (40mg/kg/2day)
C
Control
Olverembatinib
#1 #2 #3 #4 #5
D
Pancreas & spleen / body rate
NC Olverembatinib
E
Body weight (g)
NC
Olverembatinib
Treatment time (Day)
F
Olvermebatinib
p-SRC
SRC
p-AKT
AKT
p-MYC
MYC
GAPDH
G
Normal saline:i.p.
Normal saline:p.o
Olverembatinib:p.o (40mg/kg/2day)
Gemcitabine:i.p (20mg/kg/3day)
Olverembatinib:p.o (40mg/kg/2day)
Gemcitabine:i.p (20mg/kg/3day)
H
Control
Olverembatinib
Gemcitabine
Olverembatinib+ Gemcitabine
I
Pancreas & spleen / body rate
NC
Olverembatinib
Gemcitabine
Combination
J
NC
Olverembatinib
Gemcitabine
Combination
p-JAK1
JAK1
p-STAT1
STAT1
p-SRC
SRC
GAPDH

Fig.12

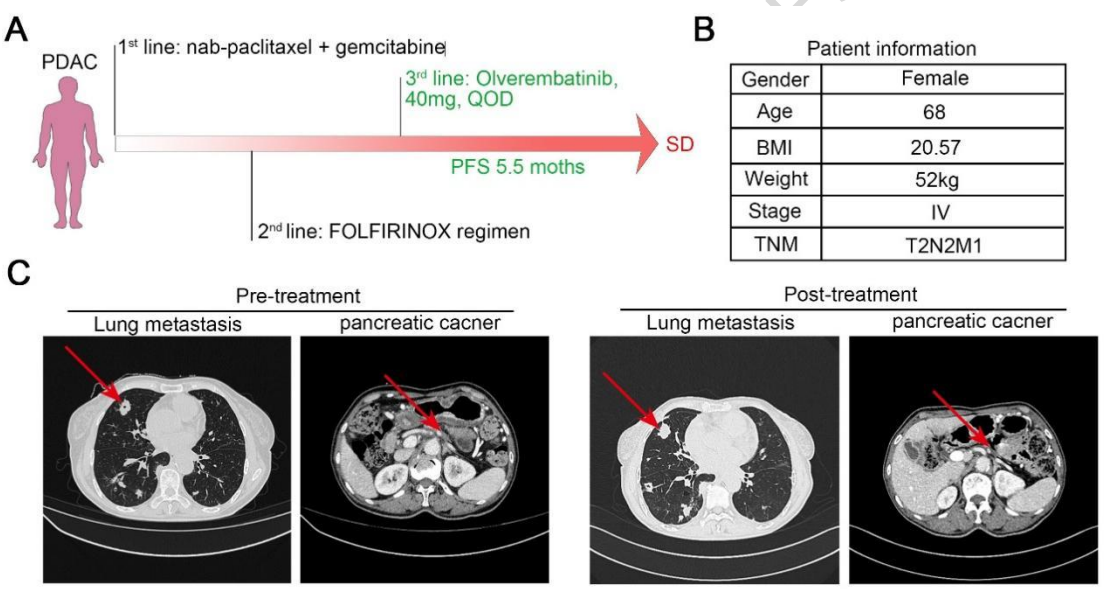
A
PDAC
1st line: nab-paclitaxel + gemcitabine
3rd line: Olverembatinib, 40mg, QOD
SD
PFS 5.5 moths
2nd line: FOLFIRINOX regimen
B
Patient information
Gender Female
Age 68
BMI 20.57
Weight 52kg
Stage IV
TNM T2N2M1
C
Pre-treatment
Lung metastasis
pancreatic cacner
Post-treatment
Lung metastasis
pancreatic cacner

Fig.13

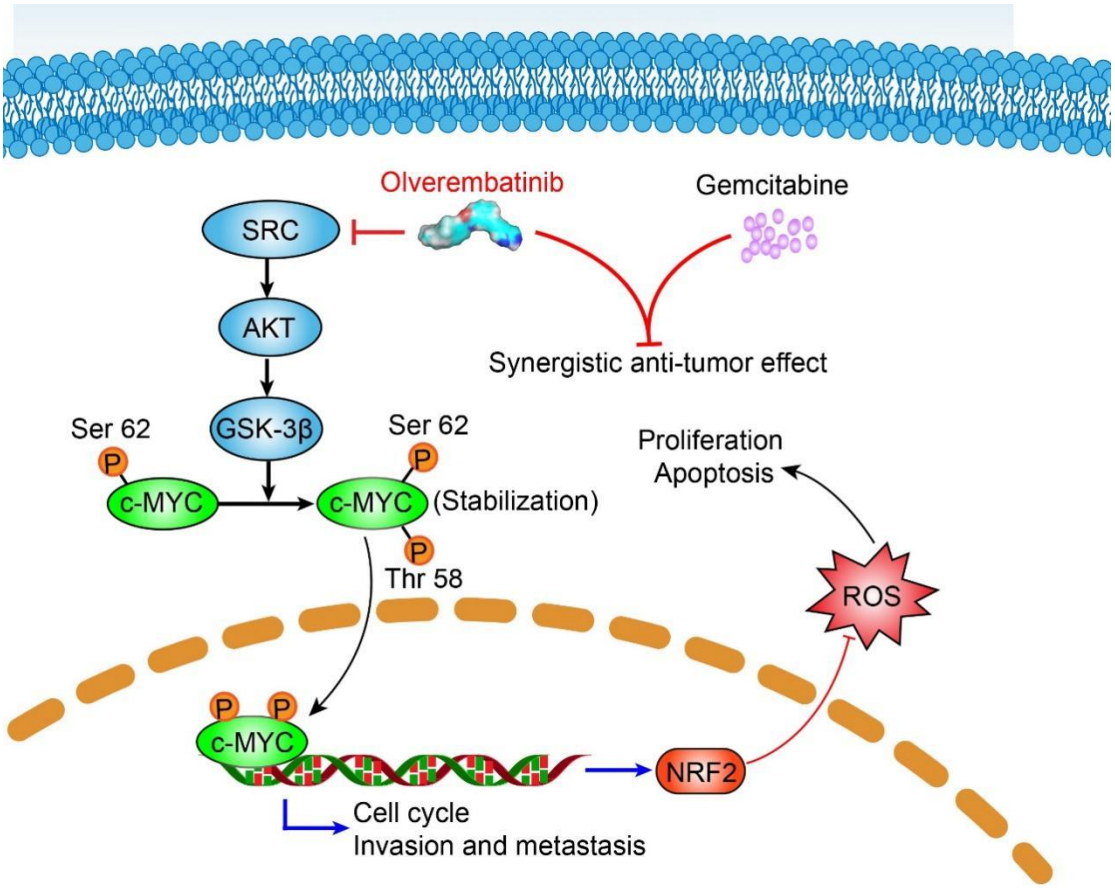
Olverembatinib
Gemcitabine
SRC
AKT
GSK-3β
Synergistic anti-tumor effect
Ser 62
Ser 62
P
c-MYC
c-MYC
(Stabilization)
Thr 58
Proliferation
Apoptosis
ROS
c-MYC
NRF2
Cell cycle
Invasion and metastasis